Table 2. Biodistribution of Radioactivity after Intravenous Injection of [^{125}I]SIB-NuB2 and [^{131}I]SIB-NuB2$_I$ in RPMI1788 Cell-Bearing SCID Mice[a]

	time after injection			
	24 h	48 h	72 h	96 h
	[^{125}I]SIB-NuB2			
blood	14.05 (1.02)	8.64 (1.18)	4.79 (1.22)	3.02 (0.39)
xenograft	4.54 (0.68)	5.36 (1.03)	3.95 (1.08)	4.81 (0.78)
liver	5.01 (0.82)	3.04 (0.39)	1.68 (0.27)	1.01 (0.10)
kidney	4.56 (0.67)	3.09 (0.50)	1.70 (0.35)	1.08 (0.22)
stomach[b]	0.33 (0.05)	0.20 (0.04)	0.38 (0.06)	0.09 (0.01)
intestine	1.15 (0.13)	1.05 (0.18)	0.58 (0.11)	0.36 (0.08)
xenograft/blood	0.32 (0.06)	0.62 (0.09)	0.83 (0.03)	1.59 (0.35)
liver/blood	0.36 (0.07)	0.35 (0.01)	0.35 (0.04)	0.33 (0.04)
	[^{131}I]SIB-NuB2$_I$			
blood	14.60 (0.57)	8.17 (1.14)	4.58 (0.72)	2.78 (0.33)
xenograft	6.20* (0.92)	7.52* (1.19)	6.04* (1.21)	7.20** (1.32)
liver	4.33 (0.49)	2.42* (0.29)	1.39 (0.10)	0.80** (0.08)
kidney	4.78 (0.71)	2.95 (0.47)	1.57 (0.18)	1.03 (0.22)
stomach[b]	0.36 (0.06)	0.20 (0.04)	0.37 (0.07)	0.08 (0.01)
intestine	1.34 (0.19)	1.03 (0.18)	0.59 (0.08)	0.35 (0.09)
xenograft/blood	0.42 (0.07)	0.92** (0.11)	1.31** (0.11)	2.59* (0.64)
liver/blood	0.30 (0.03)	0.30** (0.01)	0.30 (0.03)	0.29 (0.03)

[a] Tissue radioactivity is expressed as percent of injected dose per gram of wet tissue. Results are expressed as means (SD) of five to six animals for each point. [b] Expressed as percent injected dose. Significances determined by unpaired Student's *t*-test. *$p < 0.05$ compared to [^{125}I]SIB-NuB2. **$p < 0.01$ compared to [^{125}I]SIB-NuB2.

antibodies. It was speculated that the attachment of anchoring molecules close to an antibody molecule may cause less interaction with cell surface molecules or cell membrane of target cells, whereas attachment of linkers that place the anchoring molecules at a distance from the antibody molecule may increase nonspecific binding. We selected a butyryl-bis(aminocaproate) linkage between a maleimide moiety and an octaarginine peptide with an expectation that the octaarginine moiety would not interact directly with a cell but interact strongly after the specific binding of antibody takes place. Since the importance of the density of AR-CPP molecules in an antibody was well-documented (*10, 11*), two R_8-conjugated antibodies holding different numbers of R_8 per molecule of the antibody were prepared (Scheme 1).

The R_8 conjugation and subsequent iodination reactions did not affect the SE-HPLC profiles of NuB2 (Figure 1B). The three SIB-labeled NuB2s possessed similar immunoreactivity to the antigen-positive tumor cells (Figure 1C). However, the heavy conjugation of R_8 to NuB2 increased the bandwidth of isoelectric focusing and raised pI of the resulting NuB2$_{III}$ (Figure 1A). The reaction of R_8 derivatives and an antibody can be better understood by considering the example of a perfectly random reaction (*29*). Poisson distribution can be used to predict how the R_8 molecules will be distributed among the individual antibody molecules. According to the calculation (Figure 1D), the majority of NuB2$_I$ contained up to 2 molecules of R_8 per molecule of NuB2. On the other hand, NuB2$_{III}$ consisted of a variety of conjugates ranging from 1 to 7 R_8 molecules per molecule of NuB2 with over 65% of NuB2$_{III}$ containing more than 3 R_8 molecules per molecule of NuB2, which accounts for the wide bandwidth of the isoelectric focusing.

The effect of R_8 conjugation levels on the target cell binding was assessed using CD20 positive cells. [^{125}I]NuB2$_{III}$ exhibited high cell-bound radioactivity levels even in the presence of a 1000-fold excess of cold NuB2. Since the cell-bound radioactivity levels of [^{125}I]SIB-8E1$_{III}$ were much lower than those of [^{125}I]SIB-NuB2$_{III}$, the majority of the cell-associated radioactivity of [^{125}I]NuB2$_{III}$ would be attributable to the specific antigen binding, followed by the strong interaction of the R_8 moieties with the cell. The low cell-bound radioactivity of [^{125}I]SIB-NuB2$_I$ in the presence of excess NuB2 suggested slower interaction kinetics of R_8 moieties with the cell, following the specific binding. However, when the dissociation rates from the cells were compared, not only [^{125}I]SIB-NuB2$_{III}$ but also [^{125}I]SIB-NuB2$_I$ exhibited much longer residence times in the CD20 positive tumor cells than [^{125}I]SIB-NuB2 (Figure 2C). The confocal microscopy confirmed that both NuB2$_I$ and NuB2$_{III}$ were present on the cell membrane (Figure 2A). These studies supported the hypothesis that the conjugation of anchoring molecules that possess strong interaction with cell surface molecules or cell membrane prolonged the retention of radiolabeled antibodies on tumor cells by fixing the antigen-bound antibodies on target cells, although the binding kinetics of anchoring molecules with the cell was affected by their density. This also suggested that further improvement of spatial location of the R_8 molecule may increase the binding kinetics.

Despite favorable anchoring ability, the heavy conjugation of R_8 affected biodistribution profiles of the parental antibody. As shown in Table 1, [^{125}I]SIB-NuB2$_{III}$ displayed faster clearance from the blood and higher accumulation in the liver in normal mice, as also observed in prior studies (*30*). On the other hand, both [^{125}I]SIB-NuB2 and [^{125}I]SIB-NuB2$_I$ displayed similar biodistribution (Table 1). These results reinforced the importance of the number of R_8 molecules attached per molecule of an antibody to retain its in vivo behavior (*10, 11*) and showed that the present conjugation of up to 2 R_8 molecules per molecule of NuB2 did not induce any significant changes in biodistribution. Recently, we have observed that the biodistribution of PAMAM dendrimers is predominantly determined by their net molecular charge as measured by both zeta potential and pI values (*31*). The present study also suggests that the determination of net molecular charge of AR-CPP-modified antibodies may be useful to predict their pharmacokinetics.

The biodistribution studies in tumor-bearing SCID mice were investigated with [^{125}I]SIB-NuB2 and [^{131}I]SIB-NuB2$_I$ since they exhibited similar pharmacokinetics in normal mice. To minimize individual differences, the biodistribution studies were conducted after injection of a mixed solution of [^{131}I]SIB-NuB2$_I$ and [^{125}I]SIB-NuB2. As shown in Table 2, the role played by R_8 conjugation on tumor accumulation was clearly demonstrated in the biodistribution studies, where [^{131}I]SIB-NuB2$_I$ exhibited significantly higher radioactivity levels in the xenograft than those of simultaneously administrated [^{125}I]SIB-NuB2 with no significant increase being observed in the radioactivity levels of blood, liver, and other tissues between the two. When considering the in vitro studies, these results would be attributable to the delayed dissociation rates of [^{131}I]SIB-NuB2$_I$ from the target cells in vivo.

In conclusion, the findings in this study indicated that the conjugation of anchoring molecules to an antibody that possesses a strong interaction with cell surface molecules or cell membrane enhanced accumulation in target tissues by fixing antigen-bound antibodies on target cells. This study also showed that conjugation of up to 2 molecules of R_8 per molecule of NuB2 satisfied both target-specific binding of antibodies and strong cell binding property of R_8. Further optimization of the conjugation chemistry would be required to provide uniform conjugates with appropriate linkage structure between R_8 and an antibody. These findings strongly suggested the application of AR-CPP to enhance specific accumulation of antibodies in target for more effective RIT.

ACKNOWLEDGMENT

The authors appreciated to Immuno-Biological Laboratories Co, Ltd., for supplying the relevant and irrelevant antibodies. Y. Azuma is grateful for the JSPS Research Fellowship for Young Scientists. This work was supported in part by a Grant-in-Aid for Scientific Research (B), for Exploratory Research,

for Development of Systems and Technology for Advanced Measurement and Analysis, and by Special Funds for Education and Research (Development of SPECT Probes for Pharmaceutical Innovation) from the Ministry of Education, Culture, Sports, Science, and Technology, Japan. This work was dedicated to our distinguished colleague, the late Mr. Yuichiro Taira.

LITERATURE CITED

(1) Fisher, R. I., Kaminski, M. S., Wahl, R. L., Knox, S. J., Zelenetz, A. D., Vose, J. M., Leonard, J. P., Kroll, S., Goldsmith, S. J., and Coleman, M. (2005) Tositumomab and iodine-131 tositumomab produces durable complete remissions in a subset of heavily pretreated patients with low-grade and transformed non-Hodgkin's lymphomas. *J. Clin. Oncol. 23*, 7565–7573.

(2) Vose, J. M. (2004) Bexxar: novel radioimmunotherapy for the treatment of low-grade and transformed low-grade non-Hodgkin's lymphoma. *Oncologist 9*, 160–172.

(3) Gordon, L. I., Molina, A., Witzig, T., Emmanouilides, C., Raubtischek, A., Darif, M., Schilder, R. J., Wiseman, G., and White, C. A. (2004) Durable responses after ibritumomab tiuxetan radioimmunotherapy for $CD20^+$ B-cell lymphoma: long-term follow-up of a phase 1/2 study. *Blood 103*, 4429–4431.

(4) Witzig, T. E., White, C. A., Wiseman, G. A., Gordon, L. I., Emmanouilides, C., Raubitschek, A., Janakiraman, N., Gutheil, J., Schilder, R. J., Spies, S., Silverman, D. H., Parker, E., and Grillo-Lopez, A. J. (1999) Phase I/II trial of IDEC-Y2B8 radioimmunotherapy for treatment of relapsed or refractory CD20(+) B-cell non-Hodgkin's lymphoma. *J. Clin. Oncol. 17*, 3793–803.

(5) von Mehren, M., Adams, G. P., and Weiner, L. M. (2003) Monoclonal antibody therapy for cancer. *Annu. Rev. Med. 54*, 343–369.

(6) Goldenberg, D. M. (2001) The role of radiolabeled antibodies in the treatment of non-Hodgkin's lymphoma: the coming of age of radioimmunotherapy. *Crit. Rev. Oncol. Hematol. 39*, 195–201.

(7) Boswell, C. A., and Brechbiel, M. W. (2007) Development of radioimmunotherapeutic and diagnostic antibodies: an inside-out view. *Nucl. Med. Biol. 34*, 757–778.

(8) Jain, M., Venkatraman, G., and Batra, S. K. (2007) Optimization of radioimmunotherapy of solid tumors: biological impediments and their modulation. *Clin. Cancer Res. 13*, 1374–1382.

(9) Tempero, M., Leichner, P., Baranowska-Kortylewicz, J., Harrison, K., Augustine, S., Schlom, J., Anderson, J., Wisecarver, J., and Colcher, D. (2000) High-dose therapy with ^{90}Yttrium-labeled monoclonal antibody CC49: a phase I trial. *Clin. Cancer Res. 6*, 3095–3102.

(10) Anderson, D. C., Nichols, E., Manger, R., Woodle, D., Barry, M., and Fritzberg, A. R. (1993) Tumor cell retention of antibody Fab fragments is enhanced by an attached HIV TAT protein-derived peptide. *Biochem. Biophys. Res. Commun. 194*, 876–884.

(11) Niesner, U., Halin, C., Lozzi, L., Günthert, M., Neri, P., Wunderli-Allenspach, H., Zardi, L., and Neri, D. (2002) Quantitation of the tumor-targeting properties of antibody fragments conjugated to cell-permeating HIV-1 TAT peptides. *Bioconjugate Chem 13*, 729–736.

(12) Batra, S. K., Jain, M., Wittel, U. A., Chauhan, S. C., and Colcher, D. (2002) Pharmacokinetics and biodistribution of genetically engineered antibodies. *Curr. Opin. Biotechnol. 13*, 603–608.

(13) Goel, A., Colcher, D., Baranowska-Kortylewicz, J., Augustine, S., Booth, B. J., Pavlinkova, G., and Batra, S. K. (2000) Genetically engineered tetravalent single-chain Fv of the pancarcinoma monoclonal antibody CC49: improved biodistribution and potential for therapeutic application. *Cancer Res. 60*, 6964–6971.

(14) Boerman, O. C., van Schaijk, F. G., Oyen, W. J., and Corstens, F. H. (2003) Pretargeted radioimmunotherapy of cancer: progress step by step. *J. Nucl. Med. 44*, 400–411.

(15) Rothbard, J. B., Jessop, T. C., Lewis, R. S., Murray, B. A., and Wender, P. A. (2004) Role of membrane potential and hydrogen bonding in the mechanism of translocation of guanidinium-rich peptides into cells. *J. Am. Chem. Soc. 126*, 9506–9507.

(16) Sakai, N., Takeuchi, T., Futaki, S., and Matile, S. (2005) Direct observation of anion-mediated translocation of fluorescent oligoarginine carriers into and across bulk liquid and anionic bilayer membranes. *ChemBioChem 6*, 114–122.

(17) Nakase, I., Takeuchi, T., Tanaka, G., and Futaki, S. (2008) Methodological and cellular aspects that govern the internalization mechanisms of arginine-rich cell-penetrating peptides. *Adv. Drug Delivery Rev. 60*, 598–607.

(18) Goncalves, E., Kitas, E., and Seelig, J. (2005) Binding of oligoarginine to membrane lipids and heparan sulfate: structural and thermodynamic characterization of a cell-penetrating peptide. *Biochemistry 44*, 2692–2702.

(19) Kaplan, I. M., Wadia, J. S., and Dowdy, S. F. (2005) Cationic TAT peptide transduction domain enters cells by macropinocytosis. *J. Controlled Release 102*, 247–253.

(20) Nakase, I., Niwa, M., Takeuchi, T., Sonomura, K., Kawabata, N., Koike, Y., Takehashi, M., Tanaka, S., Ueda, K., Simpson, J. C., Jones, A. T., Sugiura, Y., and Futaki, S. (2004) Cellular uptake of arginine-rich peptides: roles for macropinocytosis and actin rearrangement. *Mol. Ther. 10*, 1011–1022.

(21) Richard, J. P., Melikov, K., Vives, E., Ramos, C., Verbeure, B., Gait, M. J., Chernomordik, L. V., and Lebleu, B. (2003) Cell-penetrating peptides. A reevaluation of the mechanism of cellular uptake. *J. Biol. Chem. 278*, 585–590.

(22) Arano, Y., Wakisaka, K., Ohmono, Y., Uezono, T., Akizawa, H., Nakayama, M., Sakahara, H., Tanaka, C., Konishi, J., and Yokoyama, A. (1996) Assessment of radiochemical design of antibodies using an ester bond as the metabolizable linkage: evaluation of maleimidoethyl 3-(tri-n-butylstannyl)hippurate as a radioiodination reagent of antibodies for diagnostic and therapeutic applications. *Bioconjugate Chem. 7*, 628–637.

(23) Percy, M. E., Baumal, R., Dorrington, K. J., and Percy, J. R. (1976) Covalent assembly of mouse immunoglobulin G subclasses in vitro: application of a theoretical model for interchain disulfide bond formation. *Can. J. Biochem. 54*, 675–87.

(24) Grassetti, D. R., and Murray, J. F., Jr. (1967) Determination of sulfhydryl groups with 2,2′- or 4,4′-dithiodipyridine. *Arch. Biochem. Biophys. 119*, 41–49.

(25) Zalutsky, M. R., and Narula, A. S. (1987) A method for the radiohalogenation of proteins resulting in decreased thyroid uptake of radioiodine. *Int. J. Rad. Appl. Instrum. A 38*, 1051–1055.

(26) Koizumi, M., Endo, K., Kunimatsu, M., Sakahara, H., Nakashima, T., Kawamura, Y., Watanabe, Y., Saga, T., Konishi, J., and Yamamuro, T. (1988) ^{67}Ga-labeled antibodies for immunoscintigraphy and evaluation of tumor targeting of drug-antibody conjugates in mice. *Cancer Res. 48*, 1189–1194.

(27) Samnick, S., Schaefer, A., Siebert, S., Richter, S., Vollmar, B., and Kirsch, C. M. (2001) Preparation and investigation of tumor affinity, uptake kinetic and transport mechanism of iodine-123-labelled amino acid derivatives in human pancreatic carcinoma and glioblastoma cells. *Nucl. Med. Biol. 28*, 13–23.

(28) Foulon, C. F., Reist, C. J., Bigner, D. D., and Zalutsky, M. R. (2000) Radioiodination via D-amino acid peptide enhances cellular retention and tumor xenograft targeting of an internalizing anti-epidermal growth factor receptor variant III monoclonal antibody. *Cancer Res. 60*, 4453–4460.

(29) Meares, C. F., and Goodwin, D. A. (1984) Linking radiometals to proteins with bifunctional chelating agents. *J. Protein Chem. 3*, 215–228.

(30) Kameyama, S., Horie, M., Kikuchi, T., Omura, T., Takeuchi, T., Nakase, I., Sugiura, Y., and Futaki, S. (2006) Effects of cell-permeating peptide binding on the distribution of ^{125}I-labeled Fab fragment in rats. *Bioconjugate Chem. 17*, 597–602.

(31) Uehara, T., Ishii, D., Uemura, T., Suzuki, H., Kanei, T., Takagi, K., Takama, M., Murakami, M., Akizawa, H., and Arano, Y. (2010) gamma-Glutamyl PAMAM dendrimer as versatile precursor for dendrimer-based targeting devices. *Bioconjugate Chem. 21*, 175–181.

BC100259Q

Current Organ Topics:

Central Nervous System Tumor
脳腫瘍
グリオーマ

Ⅱ．悪性脳腫瘍に対するホウ素中性子捕捉療法

宮武　伸一（大阪医科大学　脳神経外科）

〔*Jpn J Cancer Chemother* 38(6): 927-932, *June*, 2011〕

はじめに

ホウ素中性子捕捉療法（boron neutron capture therapy，BNCT）は原理上腫瘍に対する細胞選択的照射が可能な唯一の放射線治療法である。本稿ではBNCTの原理，悪性脳腫瘍（悪性神経膠腫と悪性髄膜腫）の治療例，治療成績，放射線壊死の治療，今後の展望等を述べていきたい。

1．BNCTの原理

BNCTは抗がん剤による化学療法と粒子線による放射線療法の双方の特徴をもつ治療法である。その原理を図1に示す[1]。まず腫瘍細胞に選択的に硼素化合物を集積させ，そこに中性子を照射する。硼素化合物には毒性はなく，治療に用いる熱もしくは熱外中性子にもほとんど細胞を壊す作用はないが，硼素原子（^{10}B）に中性子が衝突したときに発生するアルファ線とリチウム線（粒子線）ががんを破壊する。この粒子の飛距離ががん細胞1個に相当するので，硼素化合物をがん細胞に集積できれば，がん細胞のみを破壊し，硼素の入っていない正常の細胞は破壊を免れて残ることが可能となる。BNCTでがんを破壊するのは中性子ではなく，この粒子線であり，このような細胞選択的な放射線による癌の破壊はBNCT以外には存在しない。

BNCTの成否は硼素化合物の腫瘍への選択的集積と中性子の腫瘍への到達が決定する。硼素化合物の腫瘍への選択的集積は脳腫瘍の場合，以下の2点を利用して可能となる。まず使用する硼素化合物のうちBSH（sodium borocaptate）は静脈内投与により，破綻した血液脳関門（BBB）から腫瘍に受動的に集積され，正常脳ではBBBが保たれるため，BSHの集積は起こらない。今一つの化合物がBPAであり，これは必須アミノ酸であるphenylalanineを硼素で修飾した化合物である。よって蛋白代謝の亢進した腫瘍組織では能動的に集積する。この治療用化合物をフッ素ラベルしたものをトレーサーとして利用するのがF-BPA-PETである。このPETでBPAの集積が確認できれば，その腫瘍のX線に対する感受性を問わず，BNCTは必ず効果を発揮し，その適応決定および線量評価に本PETは有用である。悪性神経膠腫でのF-BPA-PETの代表例を図2Aに示す。図2Bに示すGd造影T1強調画像にほぼ一致して，この症例では対側正常脳の7倍のBPAの集積を認めた。つまり，同部位に腫瘍と正常細胞が混在しておれば，BPA単独でも，正常細胞に比べて腫瘍には7倍の粒子線が付与できることを示している。

2．悪性神経膠腫に対する治療効果

この症例はbiopsyでgrade 3以上の悪性神経膠腫と診断され，BNCTを目的に紹介された。図2にPETと造影MRIを示した。本例の治療経過を図3に示す。BNCT後1週間で大部分の造影域が消失し，この結果からも先のPETによる治療効果の予測が有用であることが確認できる。別の再発膠芽腫の症例に対するBNCT

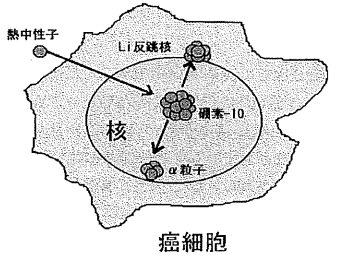

図1　BNCTの原理

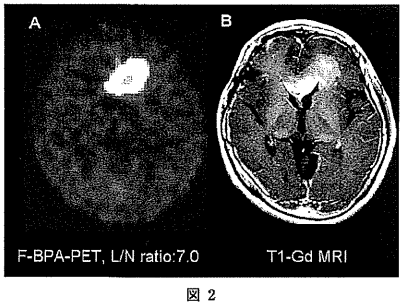

図2

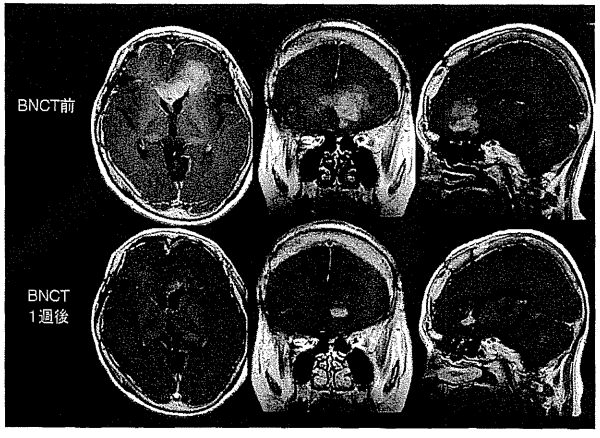

図 3

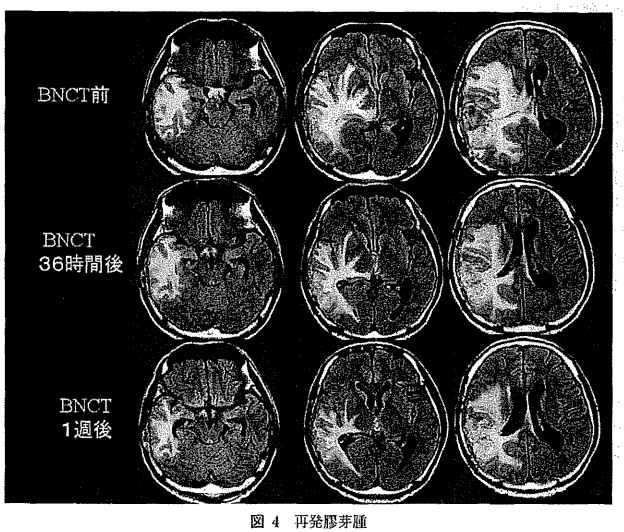

図 4 再発膠芽腫

の早期治療効果を図 4 に紹介する。この症例も 1 週間という短期間で麻痺，失語症の改善を認めた[2]。

新規診断膠芽腫における BNCT の効果を図 5 に示す。この症例は gross total resection 後，BNCT と 30 Gy の X 線外照射を加え，様子を観察している。脳放射線壊死を発症し，右上肢の麻痺が悪化したものの，テモゾロミド（TMZ）の服用なしで，5 年間再発を認めていない。

2007 年までに BNCT にて治療した新規診断膠芽腫の生存曲線を図 6 に示す。この臨床研究では明らかな再発を確認するまで，TMZ を使用していない。X 線外照射を加えた後半の 11 例の成績では，23.5 か月という生存期間中央値を示している[3]。他施設からもほぼ同様の治療成績が公表されている[4]。また，再発神経膠腫に対しても優れた腫瘍制御を経験している[5]。

3．悪性髄膜腫に対する治療効果

悪性神経膠腫とともに悪性髄膜腫も難治性悪性脳腫瘍であり，治療に難渋することも多い。図 7 に anaplastic meningioma に対する BNCT の治療例を示す。この症例は数回の手術，SRS 後に多発性に再発を認めた症例であるが，BNCT により見事に腫瘍制御が可能となり，また自立歩行も可能となった[6]。われわれは 2011 年 2 月現在で 18 例の悪性髄膜腫に本法を実施している。すべての症例で腫瘍の縮小効果を認めているが[7]，全身転移や照射外再発が問題である。

4．症候性脳放射線壊死の治療

高線量放射線治療の宿命として，脳放射線壊死が問題となる。もちろんこの放射線壊死を避けるような線量計画が重要であるが，腫瘍選択的な放射線治療である BNCT といえど，すでに放射線治療歴のある再発症例に本治療を行えば，症候性脳放射線壊死を惹起することはやむを得ない。最近，脳放射線壊死に対して，抗血管内皮増殖因子抗体であるベバシズマブ（商品名アバスチン）が著効を示すという報告がなされ[8]，われわれも積極的に使用したところ，多くの症例で著効を認めた。図 8 に BNCT 後 30 Gy の X 線照射を加えた膠芽腫の症例に発生した症候性脳放射線壊死に対するベバシズマブの効果

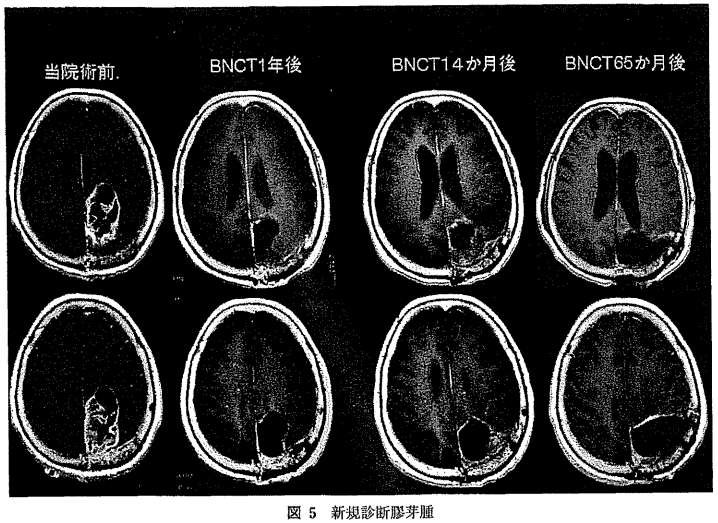

図 5 新規診断膠芽腫

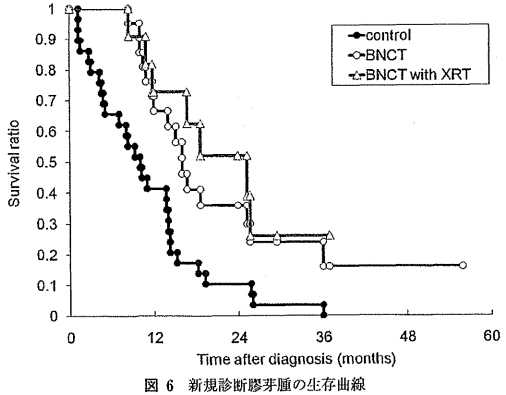

図 6 新規診断膠芽腫の生存曲線

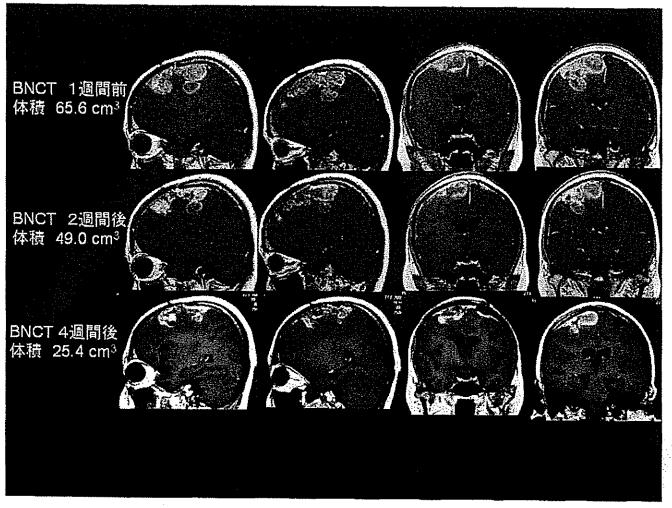

図 7 悪性髄膜腫
BNCT 待機中1か月間で腫瘍体積は2倍に急増大し，歩行不能となる。
BNCT 後1週間で歩行可能へ改善。

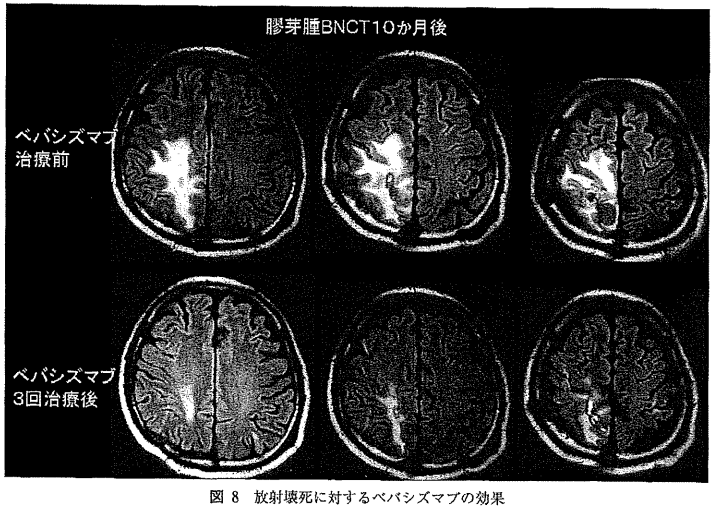

図 8 放射壊死に対するベバシズマブの効果

を示す[9]。まだ脳放射線壊死に対する保険適応のない本剤ではあるが，最近高度医療評価制度での承認が得られたので，本病態に難渋されておられれば，ぜひご相談いただきたい。

今後の展望

本稿で紹介した脳腫瘍以外にも，頭頸部がん，悪性黒色腫，難治性中皮腫等のがん腫に対して著効を示すBNCT ではあるが，一般化には大きな問題が存在する。現状で使用しうる中性子源は原子炉しか利用できない。

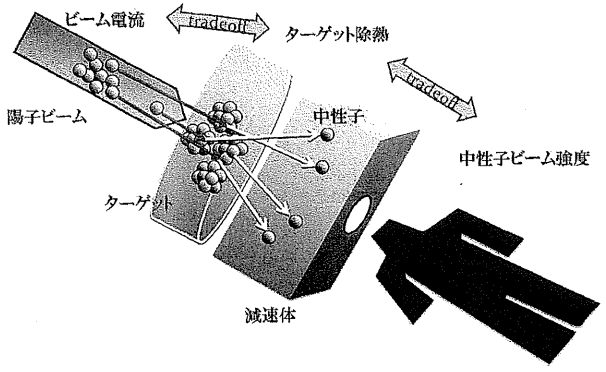

図 9 加速器中性子源

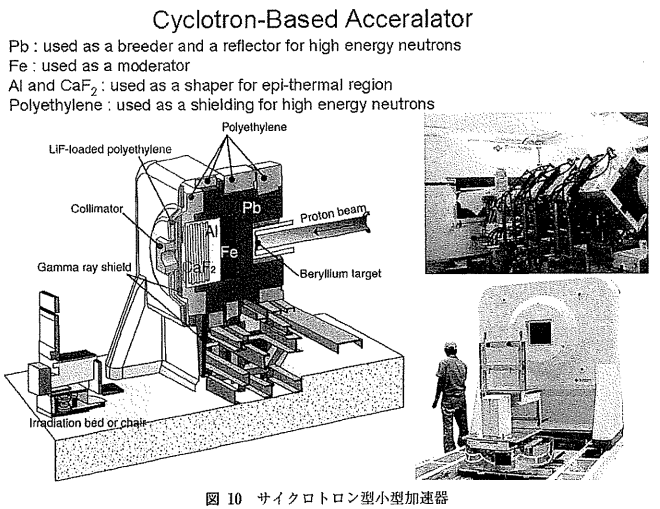

図 10 サイクロトロン型小型加速器

原子炉は広大な施設が必要であり，かつその燃料にウランを使用することにより，燃料廃棄も大きな問題となる。そこで新規中性子源として加速器が注目されている。その原理を図9に示す。陽子線を金属ターゲットに照射することによりさまざまなエネルギーの中性子が発生し，本治療に最適化したエネルギーの中性子を選別して照射に使用することができる。

ベリリウムターゲットを用い，冷却装置を工夫することにより，ターゲットの冷却という問題がクリアーでき，住友重機械がサイクロトロン型小型加速器による中性子発生装置の開発に成功した（図10）。2009年の脳腫瘍学会で実器をご案内したように，すでに必要十分な中性子を発生し，スーパー特区のサポートにより，われわれはまさに医薬品医療機器総合機構（PMDA）に治験申請を行おうとしている。

この装置を用いることにより，院内 BNCT が可能となり，本法がより一般的な治療として普及するものと期待する。

文 献

1) Coderre JA and Morris GM: Review: The radiation biology of boron neutron capture therapy. *Radiation Res* 151: 1-18, 1999.

2) Miyatake S, Kawabata S, Kajimoto Y, *et al*: Modified boron neutron capture therapy (BNCT) for malignant gliomas using epithermal neutron and two boron compounds with different accumulation mechanisms—Effectiveness of BNCT on radiographic images—. *J Neurosurgery* **103**: 1000-1009, 2005.
3) Kawabata S, Miyatake S, Kuroiwa T, *et al*: Boron neutron capture therapy for newly diagnosed glioblastoma. *J Rad Res* **50**: 51-60, 2009.
4) Yamamoto T, Nakai K, Kageji T, *et al*: Boron neutron capture therapy for newly diagnosed glioblastoma. *Radiother Oncol* **91**: 80-84, 2009.
5) Miyatake S, Kawabata S, Yokoyama K, *et al*: Survival benefit of boron neutron capture therapy for recurrent malignant gliomas. *J Neuro-Oncol* **91**: 199-206, 2009.
6) Tamura Y, Miyatake S, Nonoguchi N, *et al*: Boron neutron capture therapy for recurrent malignant meningioma. Report of first trial. *J Neurosurgery* **105**: 898-903, 2006.
7) Miyatake S, Tamura Y, Kawabata S, *et al*: Boron neutron capture therapy for malignant tumors related to meningiomas. *Neurosurgery* **61**: 82-91, 2007.
8) Gonzalez J, Kumar AJ, Conrad CA, *et al*: Effect of bevacizumab on radiation necrosis of the brain. *Int J Radiat Oncol Biol Phys* **67**: 323-326, 2007.
9) Furuse M, Kawabata S, Kuroiwa T, *et al*: Repeated treatments with bevacizumab for recurrent radiation necrosis in patients with malignant brain tumors: a report of 2 cases. *J Neuro-Oncol* (in press)

トピックス　硼素中性子捕捉療法

硼素中性子捕捉療法について

大阪医科大学脳神経外科　川端信司、松下葉子、宮田至朗、宮武伸一

1 はじめに

近年、定位放射線治療に代表される高精度放射線照射技術の開発は目覚ましく、強度変調放射線治療（Intensity modulated radiotherapy(IMRT)）やサイバーナイフ等、最先端の医療機器を使用した放射線治療が可能な施設が国内で増加している。また、動体追跡放射線治療（Image-guided radiotherapy（IGRT））は、わが国が世界に先駆けて開発した誇るべき放射線治療技術でもあり、動きのある体幹部腫瘍などに対しても空間的線量集中が可能となっている。しかしながら原発性悪性脳腫瘍である悪性神経膠腫など、明確な輪郭を持たず正常組織に浸潤性に発育する腫瘍に対しては、いかに高精度に線量集中を行っても制御は難しい。

そこで我々は、悪性神経膠腫に対する治療に、腫瘍細胞選択的粒子線治療である硼素中性子捕捉療法（Boron neutron capture therapy(BNCT)）を積極的に取り入れ臨床研究を行ってきた[1]。BNCTで利用する抗腫瘍効果は、硼素－10の中性子捕獲反応から得られる粒子線であり、粒子線治療の一種とされるが、陽子線や炭素線治療とは全く異なる原理を有した治療法である。本稿ではBNCTの最近の話題と今後の展望について紹介する。

2 BNCTの概念と適応疾患

BNCTでは、硼素化合物に与えられた腫瘍探索性と、腫瘍細胞選択照射という他の放射線治療が持ち得ない特長を生かすことにより、浸潤性に発育する腫瘍や腫瘍体積が大きくかつ形状が不整な腫瘍、既放射線治療例など、通常の放射線治療や最先端の放射線治療をもってしても適応が困難である疾患を、治療の対象とすることが可能である。

硼素（Boron、B）の安定同位体である^{10}Bは、エネルギーの低い中性子である熱中性子を高率に捕獲し、ヘリウム原子核（α粒子）とリチウム反跳核に分裂する。この反応を中性子捕獲反応という（図1）。この反応によって生じるヘリウム原子核、リチウム反跳核は、分裂後それぞれ9μm、4μmと腫瘍細胞1個に相当する飛程で動き停止し、その間に全エネルギーを放出する高LET（linear energy transfer）の粒子線であり、殺細胞効果は非常に大きい。この反応を治療に応用したのがBNCTである。あらかじめ腫瘍に集積性を有する硼素化合物を投与し、その後に中性子を患部に照射すれば、腫瘍内で生じた中性子捕獲反応により放出される高LET粒子線の飛程が腫瘍細胞の大きさを超えないため、腫瘍細胞周囲の正常組織は温存され、腫瘍細胞のみが死滅する[2]。

悪性神経膠腫、特に膠芽腫は、治療抵抗性を示すきわめて予後不良の原発性脳腫瘍である。その平均生存期間は診断から約1年とされ、過去20年間生存率に大きな改善はみられていない。その原因として血液脳関門や薬剤耐性機構の存在などが指摘されているが、最も大きな原因は腫瘍の浸潤性性格にあると言える。悪性神経膠腫の辺縁は明瞭ではなく、腫瘍細胞は画像上の造影域を越え、少なくとも周囲脳2cmまでは存在するとされる。そのため、腫瘍の造影域を外科的に全摘出行い得ても、浸潤部からの再発は必至であり、放射線・化学療法を組み合わせる必要がある。BNCTは悪性神経膠腫を最適な適応疾患として発展してきた。

3 海外におけるこれまでのBNCT

現在、本邦を中心に発展途上を遂げているBNCTであるが、臨床試験はかつて欧米でも盛んに行われた。BNCTの原理が提唱されて以後、臨床応用へ向けた開発研究が急速に進められ、1951年には医療用原子炉（ブルックヘブン国立研究所（BNL）研究炉、米国）が作られた。1953年から脳腫瘍患

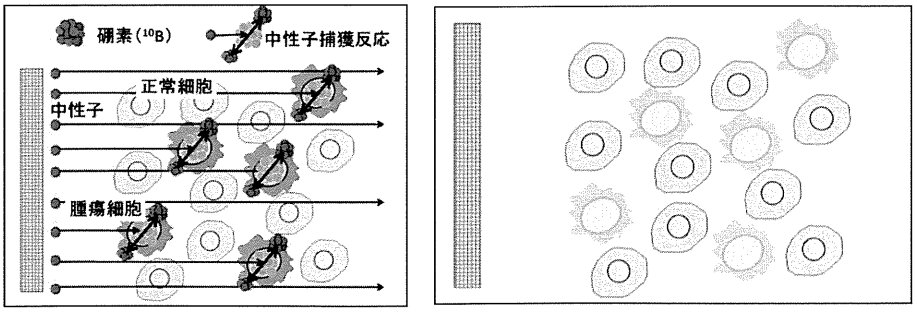

A 硼素中性子捕捉療法（BNCT）では、あらかじめ腫瘍選択性を有するホウ素（^{10}B）化合物の投与を行う。硼素（^{10}B）化合物投与後に、低エネルギーの中性子を照射することで、^{10}Bが中性子と核反応を生じ、そこから生じたヘリウム原子核（アルファ粒子）とリチウム反跳核で、腫瘍細胞を選択的に破壊する。

B この中性子捕獲反応を腫瘍細胞で選択的に生じさせることで、浸潤部においても正常細胞を温存しつつ腫瘍細胞のみが破壊される。

図1　硼素中性子捕捉療法（BNCT）における細胞選択的照射の理論図

者に対するBNCTが開始され、BNLおよびその後のマサチューセッツ工科大学炉（MITR）での臨床研究は1961年に終了し、当時のホウ素化合物が腫瘍選択性に乏しかったこと、熱中性子線の深達性が悪いことなどから、血中ホウ素濃度が高く、正常組織の障害が生じた。その後中性子線・硼素化合物に改良が行われ、米国では単剤のホウ素化合物（BPA）を用い、組織深達性で勝る熱外中性子を用いた非開頭照射が1999年まで行われた。しかし本試験での生存期間は13～15ヵ月と治療効果がわずかであり、中性子照射線量の増加を試みたところ、生存期間が延長したが深刻な中枢神経合併症が生じたため、現在米国でのBNCTは困難となっている。この米国での臨床試験には硼素化合物の投与プロトコール以外に、照射後の評価に大きな問題があったと考えられている。すなわち、当時の試験では、放射線障害・壊死の画像評価が不十分で、画像上の造影域が増大した症例がすべて再発症例と評価された結果、これをBNCTでの線量不足とみなし、線量増加が行われた可能性が高い。

欧州においは、これまでにオランダ、チェコでのBSHを用いた臨床試験、スウェーデン、フィンランドでのBPAを用いた臨床試験等がある。注目すべきは最近スウェーデンのグループが行ったBPAの投与量増量試験（900mg/kg）であり、これによってより均一に高濃度のホウ素を腫瘍に集積させる試みである[3]。2001年から2003年に本手法で新規診断膠芽腫を治療し、生存期間中央値（MST）が17.7ヵ月（N=29）と、BNLの成績（BPA（250～330mg/kg）、MST 12.8ヵ月、N=53）[4]に比較して有意に良好であった。またこの試験では、現在標準治療となった化学療法剤・テモゾロミドをBNCTに併用することで、治療成績が向上することも示している。

4 これまでの当施設での臨床経験

これまでに臨床試験で使用されてきた硼素化合物は、BSH（sodium borocaptate）と必須アミノ酸フェニルアラニンの誘導体であるBPA（boronophenylalanine）の2種類のみである。BSHは通常、血液脳関門を通過できないため、正常の脳組織には浸透しないが、悪性脳腫瘍では血液脳関門が破壊されているためにBSHが浸透し、周囲脳組織の間に硼素濃度の集積勾配が形成される。BPAはアミノ酸トランスポーターを介して、増殖の盛んな腫瘍細胞により多く取り込まれる。BPAは正常脳へも集積することや増殖の停止した休止期腫瘍細胞には取り込まれにくい弱点を有していた。我々はこれら2種類の硼素化合物を併用するプロトコールを考案し、腫瘍内の硼素分布の不均一を低減させることを試みてきた[5]。また医療照射設備の進歩から、中性子線の組織深達性は格段に改善し、現在は原子炉内での開頭手術は不要となっている。BNCTが成功するか否かは、硼素化合物の腫瘍細胞選択的集積に負うところが非常に大きい。開頭術中中性子照射を行う場合には、硼素化合物投予後に腫瘍組織を採取し、硼素の集積を実測できたが、非開頭BNCTが可能となってからは実測値が得られなくなった。照射線量は正常脳組織により規定されるが、BPAの集積はわずかながら個体差もあり、特に再発腫瘍、既放射線治療例では注意が必要となる。これを解決したのがPET検査である。BNCT用治療薬BPAを^{18}Fでラベルした^{18}F-BPAをトレーサーとした^{18}F-BPA-PET検査（**図2**）を施行することで、BNCT施行前に腫瘍と正常組織の硼素の取り込み比（Tumor/Normal brain ratio: T/N ratio）を求めることが可能である[6]。これまでの我々の解析によると、BPA-PETにおける膠芽腫のT/N比は、新規診断例で4.3、腫瘍再発例で3.9と活動性の病態においては有意差がみられず、全体でのL/N比は4.1であった。また、既放

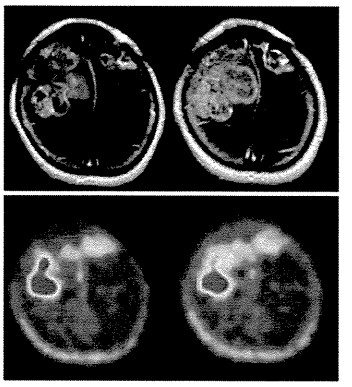

図2　硼素中性子捕捉療法施行前の^{18}F-BPA PET
再発悪性髄膜腫症例のガドリニウム造影MRI（上段）と^{18}F-BPA PET（下段）の対比を示す。本例は、複数回の定位的放射線治療を受けた後に再発を生じている。造影領域がPETトレーサーの集積に一致しないことがポイントであり、BNCTでは高集積を認める病変のみに治療効果が及び、単に過去の治療の影響から造影を受けた部位は照射されない。

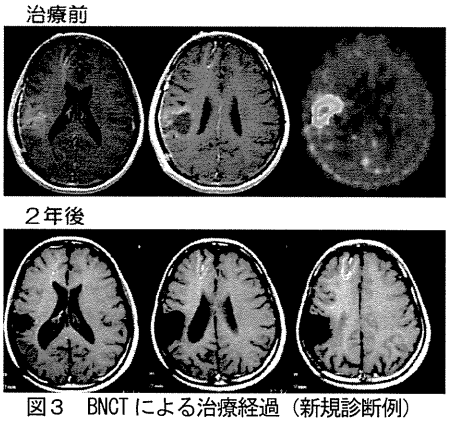

図3　BNCTによる治療経過（新規診断例）
新規診断膠芽腫症例に対して長期間の局所制御が得られている。照射前の^{18}F-BPA PETは高集積を示し、2年後のMRIでも局所再発なく経過している。

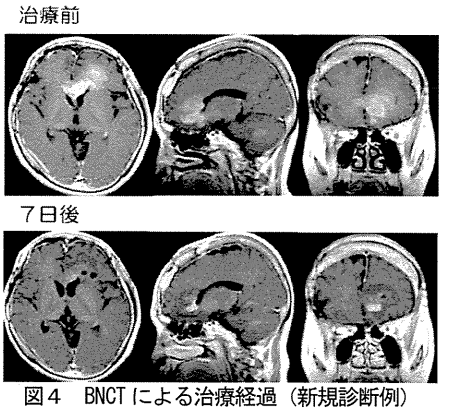

図4　BNCTによる治療経過（新規診断例）
新規診断膠芽腫症例に対して、BNCT後早期から著名な腫瘍縮小効果が得られている。

射線治療例では腫瘍再発と放射線壊死の鑑別も可能であり、本PET検査はBNCTの適応判断・治療計画のみならず治療後の病態診断に対しても有用であることがわかってきた[7]。

2007年までの新規診断膠芽腫の生存期間は、従来の開頭摘出手術＋X線分割外照射の成績を有意に上回り、BNCT治療例の生存期間中央値（MST）は15.6ヵ月（ハザード比：0.4）であった。また、既存の硼素化合物では前述の我々のプロトコールにおいても深部線量の不足、細胞レベルでの不均一性が解消されたとは言い難く、X線分割外照射の併用およびBPAの増量・長時間投与を導入し、MSTは23.5ヵ月とさらなる生存期間の延長傾向を示すことができた[8]（**図3、4**）。また最近では、YamamotoらがBNCTの自験例から、新規診断膠芽腫における開頭・術中照射群と非開頭・外照射群の治療成績を比較し報告している。これによれば、開頭・術中照射群ではBSH単剤を用い、非開頭・外照射群では我々と同様、BSH・BPA（250mg/kg）の併用にX線分割外照射を組み合わせ、MSTがそれぞれ23.3（N=7）、27.1（N=8）ヵ月と非常に良好である[9]。新規診断例におけるX線分割外照射の併用は、既放射線治療例における再照射（**図5**）と同様、腫瘍細胞選択性を有するBNCTならではの強みであり、標準治療に上乗せすることも可能な放射線治療である。BNCTの治療回数は年々増加傾向にあったが、国内2箇所の医療用原子炉（日本原子力研究開発機構4号炉（JRR4、茨城県・東海村）、京都大学原子炉実験所（KUR、大阪府・熊取町））は、共に長期間の補修・メンテナンスに入り、本邦でのBNCTは休止状態にあった。昨年になってようやくJRR4（2010年3月）、KUR（2010年6月）が再稼働し、医療照射は本格的に再開した。

5 悪性髄膜腫に対する挑戦

悪性髄膜腫は膠芽腫と同様に、周囲脳への浸潤性発育を伴う制御困難な脳腫瘍である。我々はこれまでに、悪性髄膜腫に対してもBNCTによる挑戦を行ってきた[10]。再発悪性髄膜腫12例に対して20回のBNCTを施行し、全例複数回の手術や放射線治療後の再発患者である。適応の判断にはBPA-PETを使用し、L/N比は平均3.8であった（**図2**）。初回BNCT時の最小腫瘍線量は18.8～50.7Gy-Eqと計算され、全例で腫瘍体積の縮小を認めた。BNCT後の全体の生存期間は平均15ヵ月、初発時からの生存期間は94ヵ月であった。局所制御は良好であったが、全身への転移・髄腔内播種が主な死因となった。髄膜腫は発生母地が脳表に近く、BNCT治療においては比較的有利な例が多いが、多発性に再発・増大を繰り返す例が多く、単独・単回照射での制御は困難である。我々のこれまでの治療経験から、悪性髄膜腫がBNCTに良好に反応する腫瘍群であることを示したが、再発例では既に複数回の放射線治療を受けていることが多く、今後は初回治療時にBNCTを用いることで予後の改善に期待できると考えている。

6 多施設共同第2相臨床試験について

将来的な展望として、BNCTがさらなる発展を遂げるためには、より腫瘍選択性を有する強力な硼素化合物の開発が重要な課題と指摘される。しかしながら、そもそも原子炉を用いて治療を行う限り、BNCTは臨床研究の域を脱することはできず、試薬開発にとどまる現状では、薬剤開発という創薬シーズを刺激することは困難である。そこでBNCTが

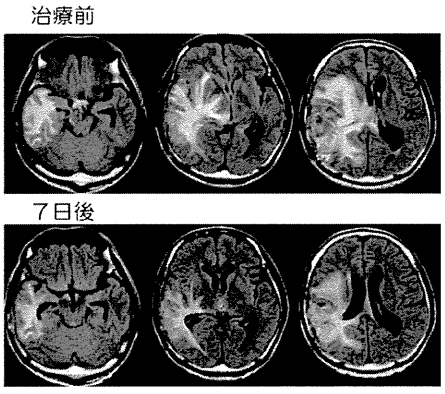

図5 BNCTによる治療経過（再発既放射線治療例）
既放射線治療、再発膠芽腫症例に対しても、BNCT後早期から脳浮腫が軽減しているのがわかる。同時に正中線変位は解消され、神経学的症状も改善が得られた。

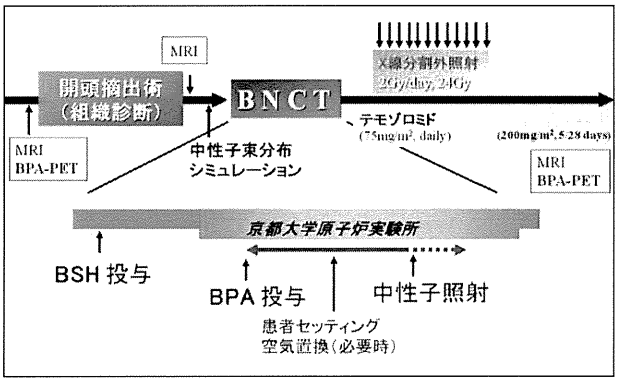

図6 原子炉BNCTによる多施設共同第2相臨床試験（進行中）のプロトコール

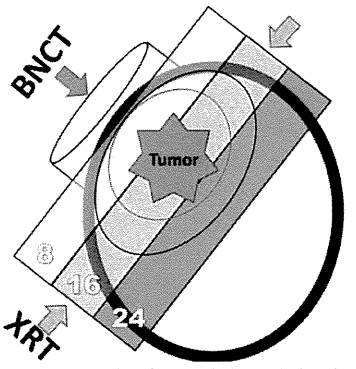

図7 BNCTとX線分割外照射併用治療の概略図

医療として認知されるには、まず原子炉から脱却しなければならない。最近、脳腫瘍での成績の向上や他臓器への応用など多方面からの注目もあり、加速器中性子源の開発研究に拍車がかかっている。医療用中性子源としての加速器が実現すれば、医療機器としての申請が可能となり、BNCTが医療承認を目指す“治験”という枠組みに参入できるようになる。現在、世界中で医療用加速器が開発研究されているが、国内では京都大学原子炉実験所内に設置されており、2010年秋の治験開始を目指し準備が進められている。

我々はその準備段階として、これまでの臨床経験をふまえた新規治療プロトコールを立案し、原子炉BNCTによる多施設共同第2相臨床試験（UMIN000002385, NCT00974987）を立ち上げ、症例登録を開始した。

本試験は、新規診断の膠芽腫を対象とし、プロトコールにはこれまでの我々の経験が集約されている（**図6**）。初発膠芽腫を対象として、主要評価項目を全生存期間、副次評価項目を腫瘍縮小効果と有害事象の発現とし、BNCT及びX線分割外照射（24Gy）（**図7**）にテモゾロミドを併用した放射線化学療法の治療効果を検討することを目的とした。登録症例の主な適格規準は次のように定めた。

1）手術により病理組織学的に膠芽腫の診断が得られている患者

2）MRI画像において、次のことが確認されている患者。A. 腫瘍がテント上、一側半球に限局し、最深部が頭皮より6 cm以内の症例（最深部が6 cm以上であっても、腫瘍摘出腔への空気置換により照射可能と判断した症例は適応とする）、B. 単発であり、播種を認めない。

3）同意取得時年齢が15歳以上75歳以下の患者

4）Karnofsky Performance Scale（KPS）が60%以上の患者

また治療のプロトコールは、1）BNCT、2）X線分割外照射：2Gy/日x12日、3）テモゾロミド併用投与（X線分割外照射終了まで75mg/m^{2}連日）、4）テモゾロミド維持療法（X線分割外照射終了後150-200mg/m^2、5日間投与23日休薬を繰り返す）で行い、2年間の患者登録の後、2年間の追跡調査を行うこととした。以上の実施計画を作成し、臨床研究情報センターに登録および参加施設間での調整を行い、本年3月から施設・症例登録を開始している。目標症例数は、第2相臨床試験であるがテモゾロミドによる標準治療との比較を視野に、これまでの我々のBNCT治療成績をもとに統計学的解析を行い、45例とした。

7 BNCTの今後

加速器BNCTが臨床応用されれば、照射の自由度は増し、現時点では困難な、分割照射や複数回照射、多門照射など様々な応用が可能となる。また今後は、動物実験でその有効性が示されている、分子標的薬やナノテクノロジー、ドラッグデリバリーシステムなどの手法を用いたホウ素化合物の臨床応用も期待される[2]。現在BNCTは、悪性脳腫瘍に加え、再発頭頸部腫瘍、多発肝腫瘍、胸膜中皮腫に対しても、その適応を拡げている状況にある。脳腫瘍はもちろん、これらの新規適応疾患に対しても、BNCTが有用な新規治療法になり得るという科学的根拠を、臨床試験を通じて明らかにする必要がある。

参考文献

1)川端信司ほか: PET journal **6**: 26-9, 2009.
2)Barth RF, et al: Clin Cancer Res **11**: 3987-4002, 2005.
3)Skold K, et al: Acta Neurol Scand, 2009.
4)Diaz AZ: J Neurooncol **62**: 101-9, 2003.
5)Kawabata S, et al: J Neurooncol **65**: 159-65, 2003.
6)Imahori Y, et al: Clin Cancer Res **4**: 1825-41, 1998.
7)Miyashita M, et al: J Neurooncol **89**: 239-46, 2008.
8)Kawabata S, et al: J Radiat Res (Tokyo) **50**: 51-60, 2009.
9)Yamamoto T, et al: Radiother Oncol **91**: 80-4, 2009.
10)Miyatake S, et al: Neurosurgery **61**: 82-90, 2007.

Applied Radiation and Isotopes 69 (2011) 1642–1645

Contents lists available at ScienceDirect

Applied Radiation and Isotopes

journal homepage: www.elsevier.com/locate/apradiso

Experimental verification of beam characteristics for cyclotron-based epithermal neutron source (C-BENS)

H. Tanaka [a,*], Y. Sakurai [a], M. Suzuki [a], S. Masunaga [a], T. Mitsumoto [b], K. Fujita [b], G. Kashino [a], Y. Kinashi [a], Y. Liu [a], M. Takada [c], K. Ono [a], A. Maruhashi [a]

[a] Research Reactor Institute, Kyoto University, Osaka 590-0494, Japan
[b] Sumitomo Heavy Industries Ltd., Tokyo 141-6025, Japan
[c] National Institute of Radiological Sciences, Chiba 263-8555, Japan

ARTICLE INFO

Available online 21 March 2011

Keywords:
Boron neutron capture therapy
Cyclotron-based neutron source
Epithermal beam
Multi-foil

ABSTRACT

A cyclotron-based epithermal neutron source has been developed for boron neutron capture therapy. This system consists of a cyclotron accelerator producing 1.1-mA proton beams with an energy of 30 MeV, a beam transport system coupled with a beryllium neutron production target, and a beam-shaping assembly (BSA) with a neutron collimator. In our previous work, the BSA was optimized to obtain sufficient epithermal neutron fluxes of $\sim 10^9$ cm^{-2} s^{-1} using a Monte Carlo simulation code. In order to validate the simulation results, irradiation tests using multi-foil activation at the surface of a gamma-ray shield located behind the collimator and water phantom experiments using a collimated epithermal neutron beam were performed. It was confirmed experimentally that the intensity of the epithermal neutrons was 1.2×10^9 cm^{-2} s^{-1}.

1. Introduction

At the Kyoto University Research Reactor Institute (KURRI), clinical trials of boron neutron capture therapy (BNCT) have been performed using the Kyoto University Research Reactor (KUR) (Sakurai and Kobayashi, 2002). The operation of KUR was stopped from March 2006 to May 2010 because of the change to low-enriched nuclear fuel. Clinical trials were restarted in May 2010.

At KURRI, a cyclotron-based neutron source (C-BENS) has also been developed for clinical use. In our previous work, a beam-shaping assembly (BSA) was optimized to obtain a sufficient intensity of epithermal neutrons, with reduction of gamma-ray contamination and of fast neutron doses (Tanaka et al., 2009). The design-based C-BENS was manufactured and installed at KURRI in December 2008. We started neutron production tests in March 2009. As of December 2010, various irradiation physical characteristics, such as whole-body exposure and measurements of BSA activities for reduction of worker exposure, and also biological characteristics, using cells and mice, had mostly been evaluated. It is especially important to confirm the influence of high-energy neutrons because the neutron energy of the C-BENS is higher than that of KUR.

In this paper, in order to validate the simulation results, irradiation tests using multi-foils for detecting high-energy neutrons over several MeV, and using a water phantom for detecting thermal neutron distributions, were performed.

2. Materials and methods

2.1. Cyclotron-based epithermal neutron source

The C-BENS consists of a cyclotron accelerator, manufactured by Sumitomo Heavy Industries, Ltd. (Tokyo, Japan), which can produce a 1.1-mA proton beam with an energy of 30 MeV, a beam transport system, a BSA, a collimator assembly (CA), and an irradiation bed. A detailed description of the device features is given in Mitsumoto et al. (2010). The schematic layout of the CA and the BSA of the C-BENS is shown in Fig. 1. The CA can move backward to view the setting position of a patient through the collimator window; this backward movement is also used to measure the neutron spectrum under free-in-air conditions in order to establish neutron sources for treatment planning.

To reduce the heat input at the beryllium target, the proton beam was expanded using scanner magnets. Reactions between 30-MeV protons and the beryllium target emit high-energy neutrons, up to 28 MeV, in the 0 degree direction. The BSA can reduce the neutron energy from around 28 MeV to the epithermal energy region because lead and iron work as moderators with inelastic cross-sections, and aluminum and calcium fluoride work as shapers, with a total cross-section, including the valley of

* Corresponding author. Tel.: +81 72 451 2468.
E-mail address: h-tanaka@rri.kyoto-u.ac.jp (H. Tanaka).

0969-8043/$ - see front matter © 2011 Elsevier Ltd. All rights reserved.
doi:10.1016/j.apradiso.2011.03.020

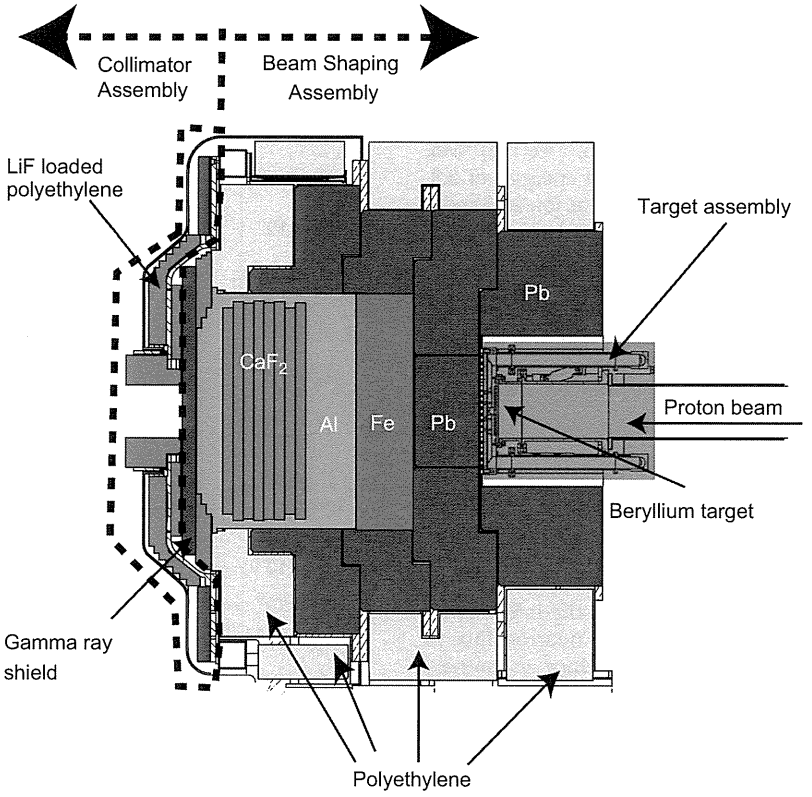

Fig. 1. Schematic layout of the beam-shaping assembly and collimator assembly of a cyclotron-based epithermal neutron source.

several tens of keV. Epithermal neutrons penetrating from the BSA go through a gamma-ray shield.

2.2. Multi-foil measurements

To measure the remaining high-energy neutrons over several MeV, multi-foils such as aluminum, nickel, and iron, which have a threshold energy, were placed at the center of the gamma-ray shield. After irradiation, the activities of the multi-foils were measured by a high-purity germanium detector (HP-Ge). To compare the results with the simulation results obtained with a MCNPX Monte Carlo code, the reaction rates for the multi-foils were derived from the equation below, using corrections such as cooling time: T_c, measuring time: T_m, and irradiation time: T; to correct the irradiation time precisely, variations in the proton current, expressed as $Q_i/\Delta t$, were taken into consideration:

$$R = \frac{\lambda C}{\varepsilon\gamma N_o e^{-\lambda t_c}(1-e^{-\lambda t_m})\sum_{i=1}^{n}\left(\frac{Q_i}{\Delta t}(1-e^{-\lambda\Delta t})e^{-\lambda(n-i)\Delta t}\right)}, \quad (1)$$

where the constants $\lambda,\varepsilon,\gamma$, and C are the decay constant, detection efficiency, gamma-ray emission ratio, and total photo-peak counts, respectively.

2.3. Water phantom measurements

To measure the dose distributions of thermal neutrons and gamma-rays in a water phantom, a $30\times30\times20$ cm cubic water phantom was set in front of a collimator of diameter 25 cm. Gold wires and cadmium-covered gold wires were installed at the central axis, to detect thermal neutron flux. TLDs were also set at the central axis. To measure the thermal neutron flux in the lateral direction, gold wires and cadmium-covered gold wires were also installed at depths of 2 and 6 cm. After irradiation, the activities of the gold wires were measured by the HP-Ge. The cadmium ratio was used to estimate the thermal neutron flux.

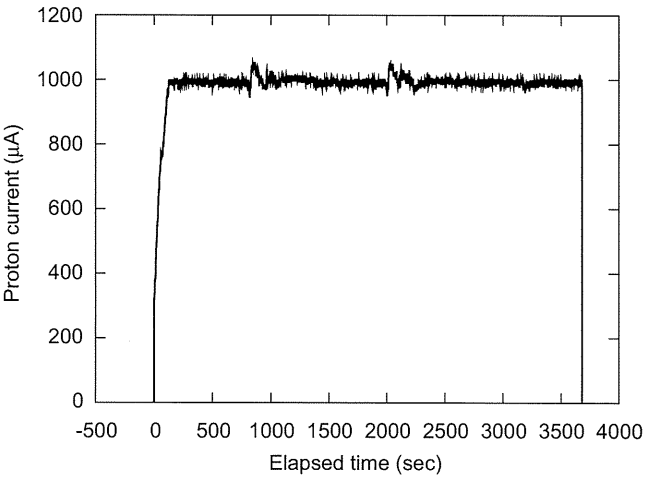

Fig. 2. Relationship between elapsed time and proton current detected at the beryllium target.

3. Results and discussion

3.1. Multi-foil measurements

Fig. 2 shows the typical relationship between elapsed time and proton current at the beryllium target. It was confirmed that the cyclotron can produce a stable proton current of up to ~1 mA for about 1 h. This is enough for use in clinical trials because the

epithermal neutron flux exceeds 10^9 cm^{-2} s^{-1} per proton current of 1 mA.

Fig. 3 shows the ratio of measured reaction rate to calculated reaction rate. Thermal/epithermal neutrons were measured by the reaction of ^{197}Au(n, γ)^{198}Au. To detect high-energy neutrons of the order of MeV, the reactions of ^{58}Ni(n,p)^{58}Co, ^{56}Fe(n,p)^{56}Mn, ^{27}Al(n, α)^{24}Na, and ^{58}Ni(n,2n)^{57}Ni with threshold energies of 2.8, 6.0, 7.2, and 13.5 MeV, respectively, were used. It was found that the ratio of the measured reaction rate to the calculated reaction rate was around 0.7 for the thermal/epithermal and high-energy regions.

According to the reference (Takata, 2010), the neutron spectra for a thick beryllium target using the cross-section data for ENDF/B-VII, and those using experimental data (Brede et al., 1989; Waterman et al., 1979), in the energy range from 17 to 35 MeV, were compared. This revealed that the cross-section data for ENDF/B-VII were higher than the experimental data. The overestimation of the cross-section data for ENDF/B-VII was a factor in the difference between the calculated and measured reaction rates.

Fig. 4 shows the relationship between the proton current at the beryllium target and the measured intensity of the epithermal neutron flux at the surface of a gamma-ray shield. This clearly confirmed good linearity between the proton current and the intensity of the epithermal neutron flux. Hence, the information on the proton current can be used to monitor neutron flux to decide on treatment times. The C-BENS can produce an epithermal flux intensity of up to 1.2×10^9 cm^{-2} s^{-1} with a proton current of 1 mA. In this paper, the energy range from 0.5 to 40 keV was defined as being the epithermal neutron range. The neutron fluxes for the thermal and fast regions were 5.0×10^6 and 6.0×10^7 cm^{-2} s^{-1}, respectively. The dose contaminations per epithermal neutron for fast neutrons and gamma-rays were 5.8×10^{-13} and 7.8×10^{-14} Gy cm^2, respectively.

3.2. Water phantom experiments

Fig. 5 shows the measured thermal neutron distribution in a water phantom compared with the calculated results. The collimator was 25 cm in diameter, which was the maximum size. The calculated

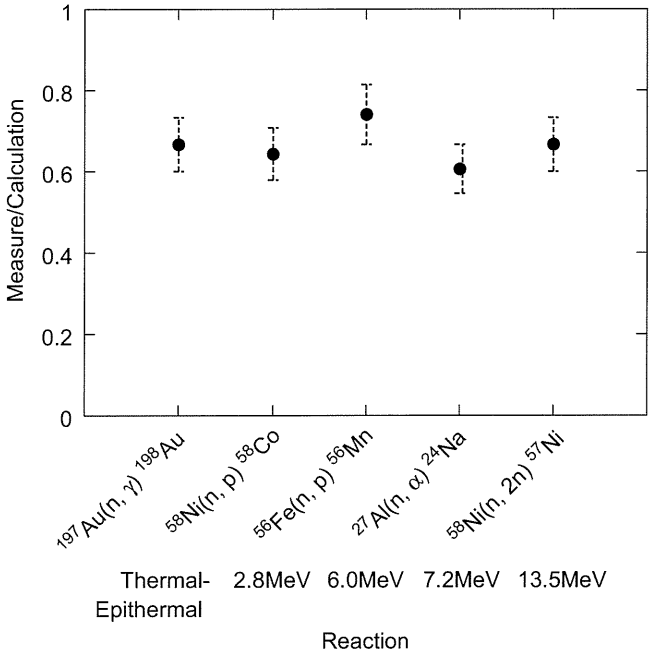

Fig. 3. Ratio of measured data from activities of multi-foils for detecting high-energy neutrons to calculated results using MCNPX.

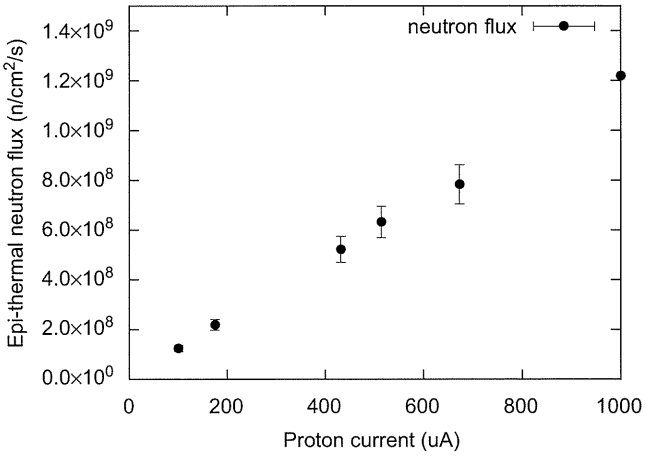

Fig. 4. Relationship between the proton current at the beryllium target and epithermal neutron flux at the surface of the gamma-ray shield.

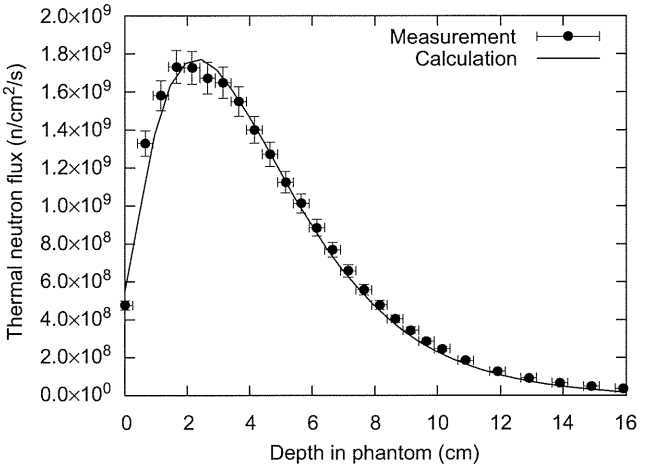

Fig. 5. Thermal neutron distributions in a water phantom at the central axis.

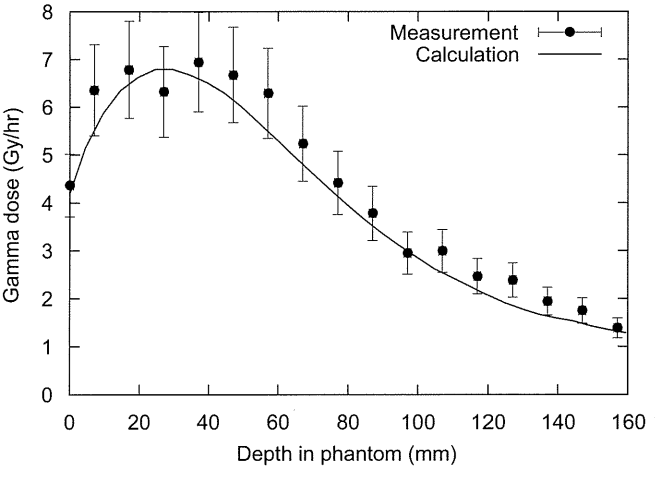

Fig. 6. Gamma-ray dose distributions in a water phantom at the central axis.

results were multiplied by the factor of 0.7 mentioned above. The calculated results multiplied by this factor were in good agreement with the measured data. The thermal neutron flux at a depth of 2 cm was 1.7×10^9 cm^{-2} s^{-1}.

Fig. 6 shows the gamma-ray dose distribution in a water phantom compared with the calculated results. The calculated

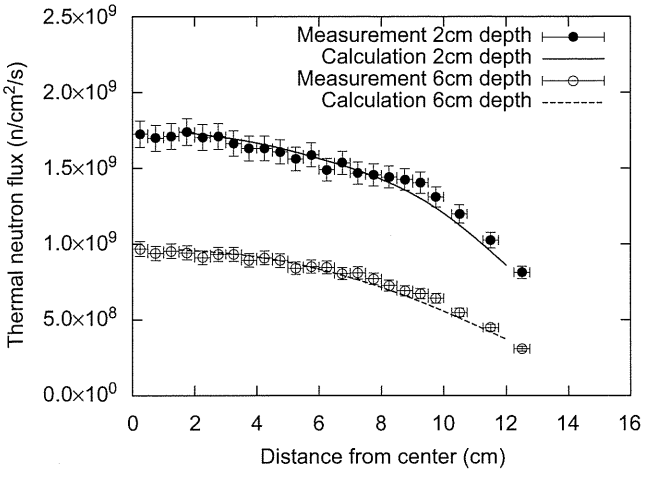

Fig. 7. Thermal neutron distributions in a water phantom in the lateral direction at depths of 2 and 6 cm.

results for the gamma-ray dose were also in good agreement with the measured data, within TLDs errors of less than 15%.

Fig. 7 shows the measured thermal neutron distribution in the lateral direction at depths of 2 and 6 cm. The measured data were also compared with the calculated results multiplied by the factor of 0.7. The calculated results were in good agreement with the measured data, except for distances beyond 8 cm from the center. It was thought that the difference between the measured data and the calculated results beyond 8 cm was caused by the effects of scattering from the walls, floor, and irradiation bed, which were not included in this calculation.

4. Conclusions

Experiments using multi-foils and a water phantom to validate the simulation results obtained with MCNPX code were performed. It was found that the simulation results for reaction rates caused by high-energy neutron and thermal neutron distributions in a water phantom were in good agreement with the measurement results. Good linearity between the proton current and epithermal neutrons at the surface of the gamma-ray shield was confirmed. Hence, the information on proton current can be used for measurements of neutron fluence in the determination of treatment times.

It was found from the experimental results that the intensity of the epithermal neutron flux at the center of the gamma-ray shield was $1.2 \times 10^9\ \mathrm{cm}^{-2}\ \mathrm{s}^{-1}$ under proton beam conditions of 1 mA. This value was about twice as large as that for the KUR reactor-based epithermal neutron source, which was used in over 300 clinical trials. Furthermore, C-BENS can produce stable operation with a proton current of 1 mA for 1 h. The use of C-BENS for clinical trials in the near future is desirable.

Acknowledgment

Part of this work was supported by the Association for Nuclear Technology in Medicine, Japan.

References

Brede, H.J., et al., 1989. Neutron yields from thick Be targets bombarded with deutrons and protons. Nucl. Instrum. Methods Phys. Res. A 274, 332–344.

Mitsumoto, T., et al., 2010. Cyclotron-based neutron source for BNCT. In: International Congress on Neutron Capture Therapy, pp. 519–522.

Sakurai, Y., Kobayashi, T., 2002. The medical-irradiation characteristics for neutron capture therapy at the heavy water neutron irradiation facility of Kyoto University Research Reactor. Med. Phys. 29 (10), 2328–2337.

Takata, T., 2010. Study on effective production of accelerator based neutron irradiation field for boron neutron capture therapy, Ph.D. Thesis, Kyoto University.

Tanaka, H., et al., 2009. Characteristics comparison between a cyclotron-based neutron source and KUR-HWNIF for boron neutron capture therapy. Nucl. Instrum. Methods Phys. Res. B 267, 1970–1977.

Waterman, F.M., et al., 1979. Neutron spectra from 35 and 46 MeV protons, 16 and 28 MeV deutrons, and 44 MeV ^{3}He ions on thick beryllium. Med. Phys. 6 (5), 432–435.

Applied Radiation and Isotopes 69 (2011) 1646–1648

Contents lists available at ScienceDirect

Applied Radiation and Isotopes

journal homepage: www.elsevier.com/locate/apradiso

Evaluation for activities of component of Cyclotron-Based Epithermal Neutron Source (C-BENS) and the surface of concrete wall in irradiation room

M. Imoto [a,*], H. Tanaka [b], K. Fujita [c], T. Mitsumoto [c], K. Ono [b], A. Maruhashi [b], Y. Sakurai [b]

[a] Graduate School of Engineering, Kyoto University, Kyoto 606-8501, Japan
[b] Research Reactor Institute, Kyoto University, Osaka 590-0494, Japan
[c] Sumitomo Heavy Industries, Ltd., Tokyo 141-6025, Japan

ARTICLE INFO

Available online 6 April 2011

Keywords:
BNCT
Activity
Identification of radioisotopes

ABSTRACT

The workers employed in BNCT must enter the irradiation room just after an irradiation under the condition of remaining activities. To reduce the radiation exposure for the workers, it is important to identify the origins of the activities. In this research, the activities induced on the concrete wall surface were evaluated using MCNP-5 and the measurement results of thermal neutron distribution. Furthermore, the radioisotopes produced in the moderator were identified with a High Purity Germanium detector. It was found that the activities of the wall were mainly caused by ^{46}Sc, ^{60}Co and ^{152}Eu, and that ^{24}Na and ^{56}Mn were mainly produced in the moderator.

1. Introduction

A new Cyclotron-Based Epithermal Neutron Source (C-BENS) was installed at Kyoto University Research Reactor Institute in December 2008. It was confirmed that the intensity of the epithermal neutron beam was about 1×10^9 cm^{-2} s^{-1}, which could be used for clinical trial of Boron Neutron Capture Therapy (BNCT). Several irradiation experiments for water phantoms, cells and mice are currently underway. To change the irradiation geometries and setups for experiments and/or BNCTs, the workers such as doctors, medical physicists, etc. have to enter the irradiation room under the condition of remaining the activities. It is assumed that the activities are originated from the components of C-BENS and the walls of the irradiation room. To reduce the radiation exposure for the workers, it is important to identify the origins of the activities.

A Monte Carlo simulation was performed to evaluate the thermal neutron distribution in the irradiation room. To confirm the validity of the simulation, the measurement of thermal neutron flux at the surface of the irradiation room was also performed. In addition, the kind of radioisotopes produced in the C-BENS component was experimentally identified using a High Purity Germanium Detector (HPGD).

2. Materials and methods

2.1. Evaluation for the concrete wall

To evaluate radioisotopes produced in the concrete wall, thermal neutron flux distribution was measured by the foil activation method using bare gold foils and cadmium-covered gold foils. The foils were placed on the surface of the concrete wall at intervals of 50 cm, as shown in Fig. 1. After an irradiation for 30 min with a proton current of 1 mA, the activities of gold foils were measured by an HPGD. Using the ratio of the activity between the bare foil and the cadmium-covered foil at the same position, the thermal neutron flux was determined.

The measured fluxes were compared with the calculation results using a Monte Carlo simulation code "MCNP-5" (Sweezy, 2008). In this calculation, the neutron spectrum at the collimator aperture, obtained from the previous work (Tanaka et al., 2009), was used. The F4, which that could derive the neutron spectrum, was placed at the same position as in the experiments. The activities in the concrete were calculated using the thermal neutron fluxes and the cross-section data for the component of the concrete. Table 1 shows the major composition of concrete (Evans et al., 1984). It was assumed that the density of the concrete was 2.1 g cm^{-3}. The cross-section data was obtained from the nuclear data library of ENDF/B-VII (Oblozinsky and Herman, 2006) and "Table of Isotopes" (Firestone, 1996).

In addition, the simulation was also performed in the case of shielding the concrete wall surface to reduce the activities caused by thermal neutrons. We selected a silicone rubber containing 20 wt% B_4C with the thickness of 1 cm as a shielding material.

* Corresponding author. Tel.: +81 72 451 2604.
E-mail address: masayuki.imoto@gmail.com (M. Imoto).

0969-8043/$ - see front matter © 2011 Elsevier Ltd. All rights reserved.
doi:10.1016/j.apradiso.2011.03.018

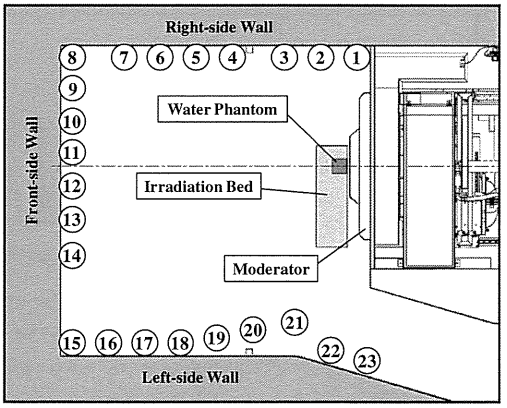

Fig. 1. Schematic layout in the irradiation room for the activation experiments. The numbers represent the positions of the gold foils. A water phantom was placed at the collimator aperture during the irradiation.

Table 1
Major element of concrete. Density of the concrete is assumed to be 2.1 g cm^{-3}.

Element	Composition (ppm)
Si	168,000
Ca	183,000
Sc	6.5
Fe	39,000
Co	9.8
Eu	0.55

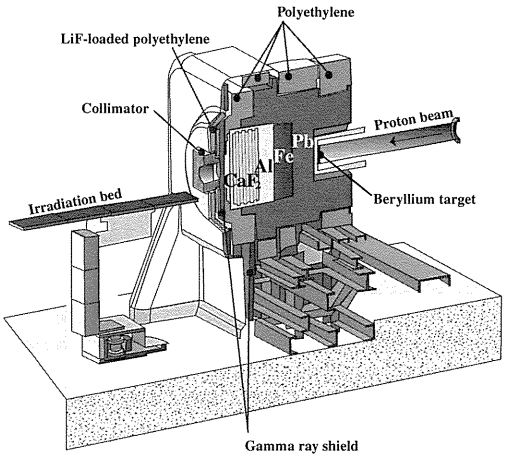

Fig. 2. Schematic layout of the moderator of C-BENS, which is constructed of Fe, Al, CaF_2 and Pb.

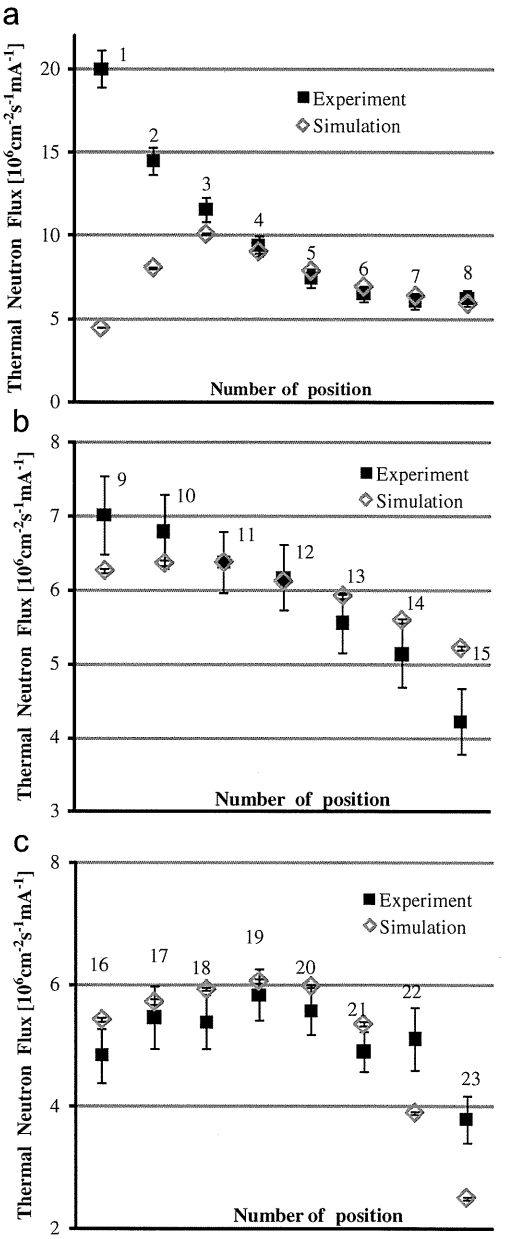

Fig. 3. Comparisons of the thermal neutron distribution on the surface of concrete wall between the calculation results and measured data. The labels represent the position numbers for (a) right-side, (b) front-side and (c) left-side wall.

2.2. Evaluation for the moderator

The kind of the radioisotopes produced in the moderator of the C-BENS was identified using an HPGD. The moderator is constructed of Fe, Al, CaF_2 and Pb as shown in Fig. 2. To prevent the event saturation caused by the background except for the objective, the HPGD was surrounded by gamma-ray shield formed by lead blocks with the collimation of 5 mm^2. The detector was brought into the irradiation room 20 min after an irradiation.

3. Results and discussions

3.1. Evaluation for the concrete wall

The comparisons of the thermal neutron distribution between the calculation results and measured data were shown in Fig. 3. In this figure, the numbers correspond to the evaluation position shown in Fig. 1. The calculation results were in good agreement with the measured data, except for some points. On the right-side wall near the collimator, the measured values were larger than the calculated values. It is suspected that the neutrons generated at the target and the beam line were reflected in the wall and leaked from the gap between the moderator and the concrete walls. This gap should be filled using shielding material such as polyethylene, etc. The calculation result of the thermal neutron flux for the 3rd position was the highest among the evaluation positions except for the leakage from the gap. Hence, the value of thermal neutron flux at the 3rd position was used for calculating the activities of the concrete wall.

Fig. 4 shows the typical neutron spectrum on the surface of concrete wall located at the 3rd and 11th positions. It is clear that thermal neutrons largely contribute to the activation of concrete wall. Based on the operation pattern of the C-BENS, the relationship

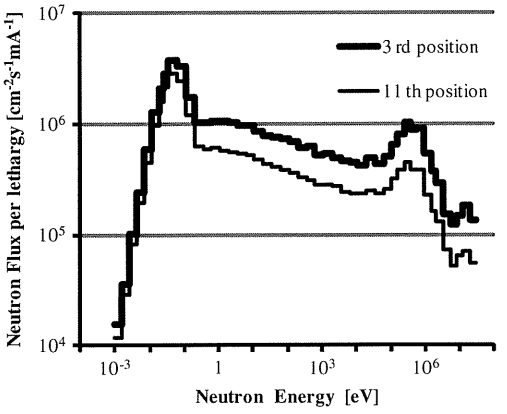

Fig. 4. Typical neutron spectrum on the surface of concrete wall located at the 3rd and 11th positions shown in Fig. 1.

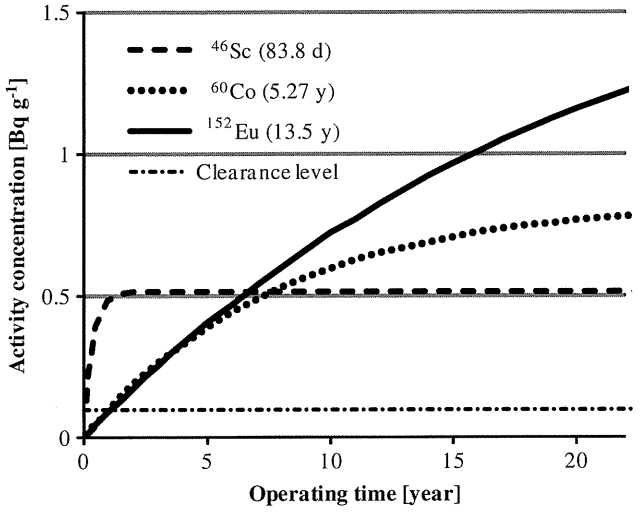

Fig. 5. Relationship between the elapsed time and the activities at the 3rd position located at the right-side wall near the collimator.

between the activities on the surface of concrete wall and elapsed time was estimated. Fig. 5 shows that the activities of the three radioisotopes such as ^{46}Sc, ^{60}Co and ^{152}Eu, exceed the IAEA clearance level of 0.1 Bq g^{-1} in less than 2 years without thermal neutron shield. On the other hand, using a silicone rubber as a thermal neutron shield, we confirmed that the activities of ^{152}Eu could be kept below the clearance level for 10 years, and those of ^{46}Sc and ^{60}Co could be kept below for more than 60 years as shown in Fig. 6.

3.2. Evaluation for the moderator

It was found that most of the activities 20 min after an irradiation were caused by ^{24}Na and ^{56}Mn. These radioisotopes can be generated from ^{27}Al(n,α)^{24}Na or ^{23}Na(n,γ)^{24}Na and ^{56}Fe(n,p)^{56}Mn or ^{55}Mn(n,γ)^{56}Mn. The isotopes such as ^{23}Na and ^{55}Mn are included in the component of C-BENS, just as impurity elements. The moderator of C-BENS consists of lead, iron, aluminum and calcium fluoride, and the isotopes such as ^{27}Al and ^{56}Fe are abundantly included. Therefore, it was concluded that the

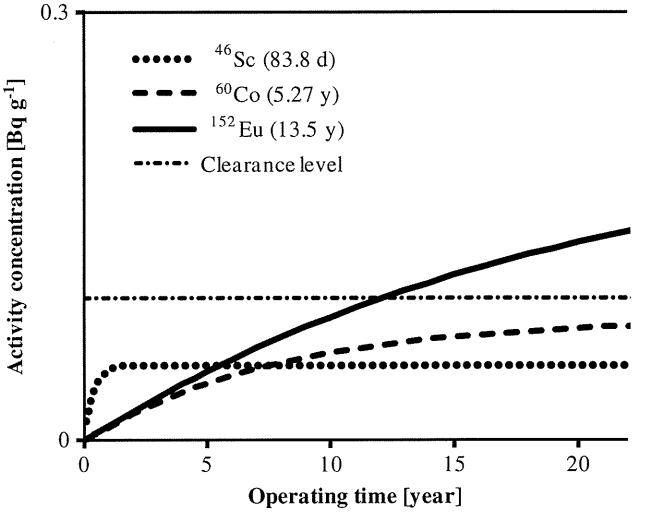

Fig. 6. Relationship between the elapsed time and the activities at the 3rd position located at the right-side wall near the collimator using thermal neutron shield.

radioisotopes such as ^{24}Na and ^{56}Mn were produced mainly due to the reactions such as ^{27}Al(n,α)^{24}Na and ^{56}Fe(n,p)^{56}Mn, respectively.

4. Conclusions

The activities induced at the surface of concrete wall of BNCT irradiation room were evaluated. Thermal neutron flux at the surface of concrete wall was determined by the gold foil activation method and simulation using MCNP-5. The activities were calculated using the cross-section data of ENDF/B-VII and the composition data of concrete. It was shown that the activities will exceed the IAEA clearance level of 0.1 Bq g^{-1} in less than 2 years without thermal neutron shield. However, the activities would have been below the clearance level for 10 years if the wall surface was shielded by silicone rubber containing 20 wt% B_4C with the thickness of 1 cm.

The kind of radioisotopes produced in the moderator of the C-BENS was identified using an HPGD surrounded by lead gamma-ray shield. It was found that most of the activities 20 min after an irradiation were caused by ^{27}Al(n,α)^{24}Na and ^{56}Fe(n,p)^{56}Mn. We found that the activities of the component of C-BENS were much higher than that of the concrete wall and these influence a radiation exposure for the workers. In the future work, quantitative estimation of the activities of the moderator of C-BENS will be performed.

References

Evans, J.C., et al., 1984. Long-Lived Activation Products in Reactor Materials. Nureg/CR, 3474.
Firestone, R.B., 1996. Table of Isotopes. eighth ed. In: Singh, B. (Ed.), Table of Isotope Data, vol. II. John Wiley & Sons, Inc., New York, p. 1554.
Oblozinsky, P., Herman, M., 2006. Evaluated Nuclear Data file ENDF/B-VII.0. Nuclear Data Sheets vol. 107 (issue 12), 2931–3118.
Sweezy, Jeremy E., 2008. MCNP—A General Monte Carlo N-Particle Transport Code, Version 5.
Tanaka, H., et al., 2009. Characteristics comparison between a cyclotron-based neutron source and KUR-HWNIF for boron neutron capture therapy. Nuclear Instruments and Methods in Physics Research B 267, 1970–1977.

Applied Radiation and Isotopes 69 (2011) 1657–1659

Contents lists available at ScienceDirect

Applied Radiation and Isotopes

journal homepage: www.elsevier.com/locate/apradiso

The optimization study of Bonner sphere in the epi-thermal neutron irradiation field for BNCT

H. Ueda [a,*], H. Tanaka [b], A. Maruhashi [b], K. Ono [b], Y. Sakurai [b]

[a] Department of Nuclear Engineering, Kyoto University, Yoshida Honmachi, Sakyo-ku, Kyoto 606-8501, Japan
[b] Research Reactor Institute, Kyoto University, Asashiro-nishi 2-1010, Kumatori-cho, Osaka 590-0494, Japan

ARTICLE INFO

Available online 2 February 2011

Keywords:
Bonner sphere
Epi-thermal neutron irradiation field
Spectrum measurement
Boric acid solution

ABSTRACT

The optimization study on the Bonner sphere in the epi-thermal neutron irradiation field for BNCT was done for the moderator material, moderator size, and activation foils as a neutron detector in the sphere. The saturated activity for the activation foil was obtained from the calculated response, and the effective energy range for each Bonner sphere was determined from the saturated activity. We can see that boric acid solution moderator is suitable for the spectrum measurement of a epi-thermal neutron irradiation field.

1. Introduction

The neutron energy of epi-thermal neutron irradiation field for BNCT covers a wide energy range. It is necessary to evaluate the neutron dose for a certain neutron-energy, because the physical property and the biological effectiveness greatly vary according to the neutron energy. Thereby, it is important to obtain the detailed information for the neutron energy spectrum before the clinical use.

In Kyoto University Research Reactor Institute (KURRI), a new BNCT irradiation system, Cyclotron-Based Epithermal Neutron Source (C-BENS), was installed in December 2008 (Tanaka et al., 2009). The several evaluations for the irradiation characteristics of this system are currently underway.

The Bonner-sphere method is one of the effective methods for the detailed evaluation of neutron energy spectrum. This method is applied for the spectral evaluation of C-BENS. Some activation foils are used as the neutron detector, and some neutron moderators are used as the sphere-wall material. For the optimization of Bonner sphere, simulation calculations for the Bonner sphere response were performed. In this paper, the optimization study on the Bonner sphere is reported.

2. Materials and methods

2.1. Bonner sphere

Bonner sphere consists of a spherical neutron-moderator shell and neutron detector placed in the sphere center. The incident epi-thermal neutron on a Bonner sphere is moderated through the moderator to thermal neutron, which is easy to detect by a kind of neutron detectors. Using the various sizes of Bonner spheres, it is possible to determine the detailed neutron spectra for the wider energy range.

In this study, activation foil was used as a neutron detector for the Bonner sphere. Indium (In), gold (Au), manganese (Mn), copper (Cu) and iron (Fe) were selected as the activation-foil materials. Water, water including boron-10, polyethylene, and graphite were selected as the neutron moderators, and the sphere diameters were changed from 5 to 20 cm for 5-cm increments. These optimized combinations were determined for the epi-thermal neutron irradiation field.

The specific saturated activity A_i^{nucl} [$g^{-1}\,s^{-1}$] using the i-th Bonner sphere is obtained from the measurement data. The superscript *nucl* represents the nuclide activated in the activation-foil, such as ^{197}Au, ^{63}Cu, etc. The saturated activity is approximately expressed in the following equation:

$$A_i^{nucl} = \sum_j R_{ij}^{nucl}\phi_i \quad (1)$$

where ϕ_i [$cm^{-2}\,s^{-1}$] is neutron flux for the j-th energy group, and R_{ij}^{nucl} [$cm^2\,g^{-1}$] is the response of the activated nuclide in unit mass of activation foil to neutron flux of the jth energy group (Awschalom and Sanna, 1985).

2.2. Irradiation system

The neutron energy spectra of the C-BENS irradiation system were calculated for some annular sources for the beam centerline. The calculated spectra are shown in Fig. 1. The vertical axis corresponds to neutron flux per a cyclotron beam-current at 1 mA. In the optimizing simulation, the spectrum in the annulus

* Corresponding author. Tel./fax: +81 72 451 2604.
E-mail address: haruaki@physics.mbox.media.kyoto-u.ac.jp (H. Ueda).

0969-8043/$ - see front matter © 2011 Elsevier Ltd. All rights reserved.
doi:10.1016/j.apradiso.2011.01.034

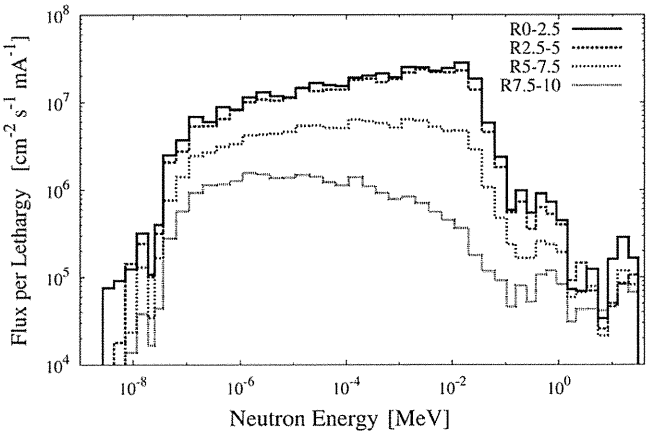

Fig. 1. Energy spectra of the epi-thermal neutron beam of C-BENS using 5-cm-radius collimator aperture. "R0-2.5" represents the annulus of 0-cm inner-radius and 2.5-cm radius.

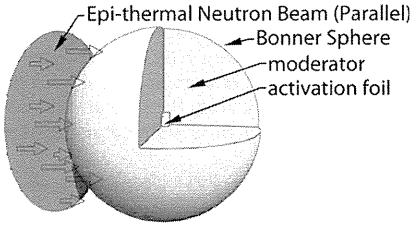

Fig. 2. Calculation geometry for the Bonner sphere response.

R0-2.5 of 0-cm inner-radius and 2.5-cm outer-radius, namely the circle of 2.5-cm radius, was considered as the representative spectrum for the C-BENS irradiation system.

2.3. Optimization of Bonner sphere

The survey calculations were performed for the responses, R_{ij}^{nucl}, for the combinations of the foils, the moderators and the sphere diameters. In the calculations, a Monte Carlo simulation code MCNP-4C2 was used (Breismeister, 2000). The calculation geometry is shown in Fig. 2. It was assumed that the directionality of the epi-thermal neutron beam was parallel and the intensity distribution on the source surface was homogeneous. The saturated activity for the C-BENS irradiation system was calculated for each energy bin, using the obtained response. The optimized energy range for each Bonner sphere was decided.

3. Results and discussions

3.1. Optimized combinations of Bonner sphere

The calculated normalized responses of ^{197}Au for the Bonner sphere using every moderator material are shown in Figs. 3–8. The saturated-activities of ^{197}Au for the C-BENS irradiation system, calculated on the assumption of the R0-2.5 spectra, are shown in Fig. 9.

On the optimization, two following points were considered. First, from Eq. (1), it is better to use the various Bonner spheres with the different normalized response functions ($R_{ij}^{nucl}/\sum_j R_{ij}^{nucl}$) for the neutron detection of the wider energy range. Second, the Bonner sphere is unavailable for the measurement of the energy range in which the saturated activity is too low to be submerged by the error. For example, in Fig. 9, 20-cm-diameter Bonner

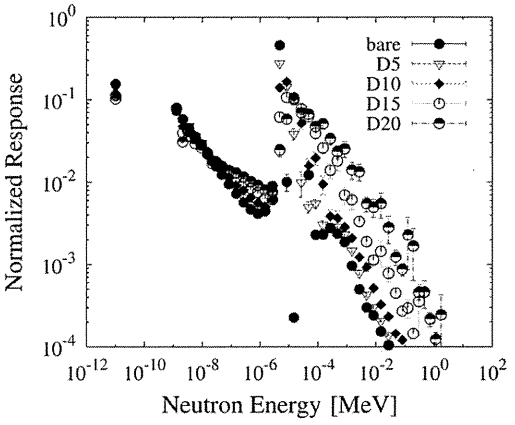

Fig. 3. Calculated normalized responses of ^{197}Au for the Bonner sphere using graphite. "D10" represents the 10 cm-diameter Bonner sphere, and "bare" corresponds to the case without the moderator sphere.

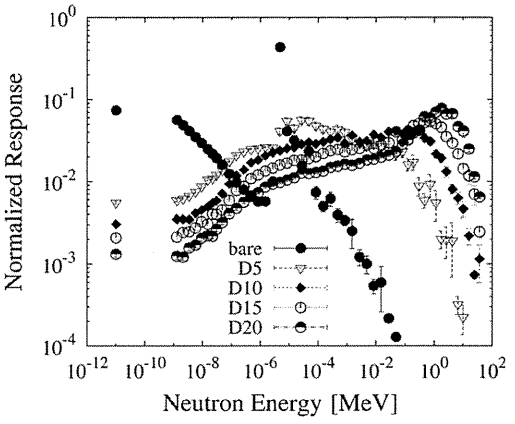

Fig. 4. Calculated normalized responses of ^{197}Au for the Bonner sphere using polyethylene.

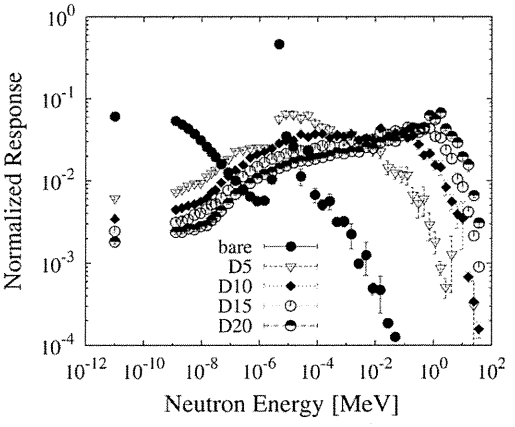

Fig. 5. Calculated normalized responses of ^{197}Au for the Bonner sphere using water.

sphere using water including ^{10}B of 1 wt% is useful for higher energy region measurement, not for lower.

According to these points, the combinations of the Bonner sphere were determined for the neutron energy region. The response functions for the following three moderators, such as water, polyethylene, and boric acid solution with boron-10 of less than 0.1 wt%, were very similar. It was considered that the Bonner spheres with these moderators make almost the same response.

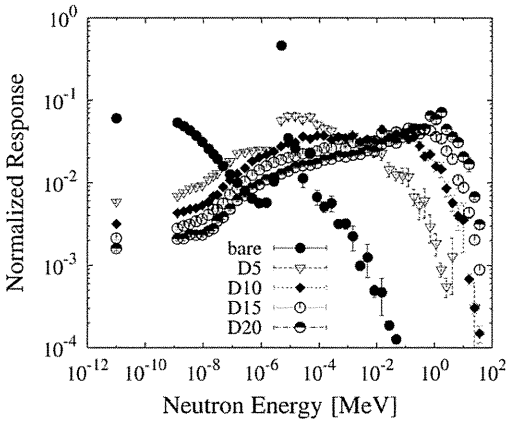

Fig. 6. Calculated normalized responses of ^{197}Au for the Bonner sphere using water including ^{10}B of 0.01 wt%.

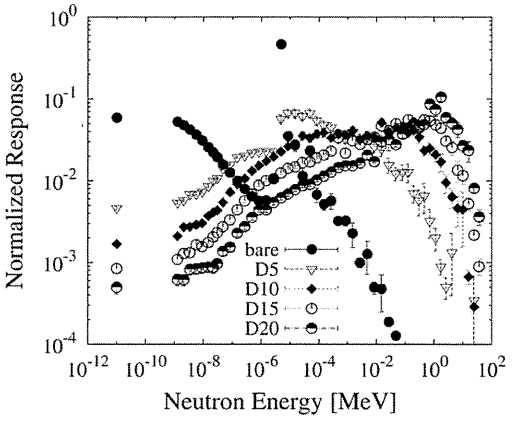

Fig. 7. Calculated normalized responses of ^{197}Au for the Bonner sphere using water including ^{10}B of 0.1 wt%.

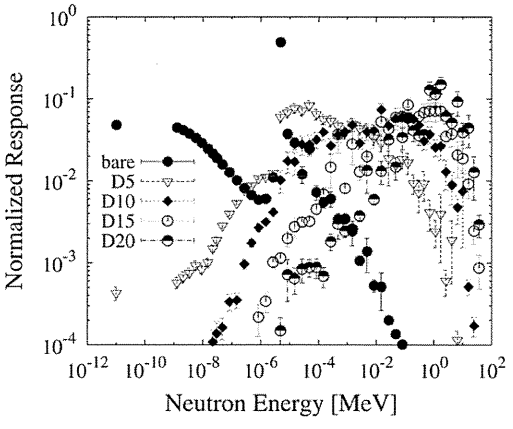

Fig. 8. Calculated normalized responses of ^{197}Au for the Bonner sphere using water including ^{10}B of 1 wt%.

The optimized combinations for the three neutron-energy-regions, such as thermal (−0.5 eV), epi-thermal (0.5 eV 40 keV) and fast neutron-regions (40 keV), are as follows.

As the moderator material, water and/or boric acid solution with boron-10 of more than 0.1 wt% are suitable for the three neutron-energy-regions. For the activation foil, Mn, Cu and/or Fe are suitable for the thermal neutron region, and In, Au, Mn, Cu and Fe are suitable for the epi-thermal neutron region. For the fast neutron region, it is the most suitable activation foil, as the threshold reaction of 115In(n, n)115*In, can be applied.

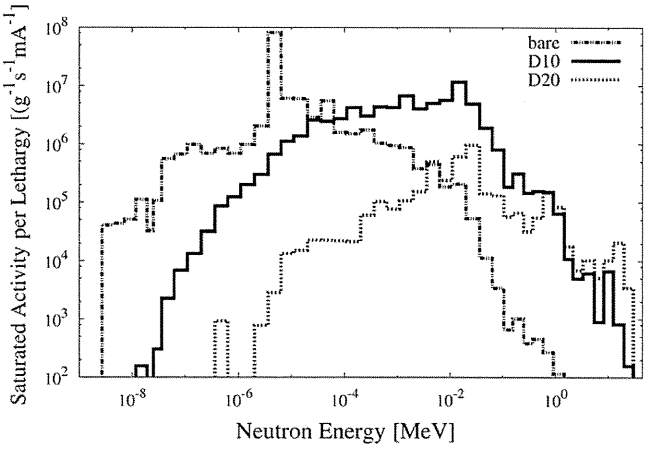

Fig. 9. The saturated-activities of ^{197}Au, calculated on the assumption of the RO-2.5 spectra, for the Bonner sphere using water including ^{10}B of 1 wt%. "D10" represents the 10-cm-diameter Bonner sphere, and "bare" corresponding to the case without the sphere.

3.2. *Boric acid solution moderator*

In this study, we found that boric acid solution with ^{10}B of more than 0.1 wt% is suitable moderator material for the wide energy range measurement. We can easily change the response function of Bonner sphere with the various concentrations of boric acid solution moderator. Boric acid solubility is 47.2 g/l at 20 °C (IUCLID Dataset, 2000). It corresponds to boric acid solution with ^{10}B of about 0.15 wt%. But, we can increase weight percent of ^{10}B with ^{10}B enrichment of natural boron.

4. Conclusions

The optimized combination for the Bonner sphere was determined for the spectral evaluation of the C-BENS neutron beam. For the evaluation in the thermal neutron energy range, Mn, Cu and Fe are suitable as the activation foil. For the evaluation in the epi-thermal range and higher energy range to 1 MeV, water moderator with the diameter of more than 20 cm is suited. And, each of the activation foils of In, Au, Mn, Cu and Fe can be used. Boric acid solution is suitable as the moderator for the wide energy range. Especially, responses of Bonner spheres with boric acid solution moderator are easy to change increasing ^{10}B concentration.

References

Awschalom, M., Sanna, R., 1985. Applications of Bonner Sphere Detectors in Neutron Field Dosimetry. Radiat. Prot. Dosimetry 10, 89–101.

Breismeister, F., 2000. MCNP—A General Monte Carlo N-Particle Transport Code. Version 4C, LA-13709-M. Los Alamos National Laboratory.

IUCLID Dataset, 2000. Boric acid, crude natural, containing not more than 85 per cent of H3BO3 calculated on the dry weight. 10043-35-3. European Commission, European Chemicals Bureau.

Tanaka, H., Sakurai, Y., Suzuki, M., Takata, T., Masunaga, S., Kinashi, Y., Kashino, G., Liu, Y., Mitsumoto, T., Yajima, S., Tsutsui, H., Takada, M., Maruhashi, A., Ono, K., 2009. Improvement of dose distribution in phantom by using epithermal neutron source based on the be (p,n) reaction using a 30 MeV proton cyclotron accelerator. Applied Radiation and Isotopes 67, S258–S261 13th International Congress on Neutron Capture Therapy BNCT: A New Option Against Cancer.